UNIVERSIDADE DE LISBOA
FACULDADE DE CIÊNCIAS
DEPARTAMENTO DE FÍSICA

Granular Electrostatics and the Formation of Aggregates

André Filipe Valente Matias

Mestrado em Física
Especialização em Física da Matéria Condensada e Nanomateriais

Dissertação orientada por:
Prof. Dr. Nuno Araújo

2018

Acknowledgments

I would like to thank Nuno Araújo, for introducing me to the topic of soft-matter physics, in particular the topic of granular matter, and also for his hard work, astonishing persistence and for providing me the opportunity to grow as a physicist.

I would like to thank Troy Shinbrot for guiding me during my stay in Princeton and Rutgers University. I also thank Sundar Sundaresan and Jari Kolehmainen for helpful discussions.

I would also like to thank Gonçalo Antunes, Luís Rebelo, Cristovão Dias, André Nunes and Diogo Pinto for their helpful input. The last thank is towards my family, in particular my parents and my brother for the continuous support and the occasional simple, but challenging, question.

I would like to acknowledge the financial support from the Luso-American Development Foundation (FLAD), FLAD/NSF, Proj. 273/2016.

Abstract

Industrial as well as natural aggregation of fine particles is believed to be associated with electrostatics. Industrially aggregation leads to profound problems, for example producing variations in active ingredient concentrations in common pharmaceuticals or manufacturing shut-downs to scour the aggregates. In nature, electrostatic aggregation can help solve the problem of planetesimal formation in a size regime where gravity and sticking forces are too weak to promote the growth of the aggregates. Yet like charges repel, so it is unclear how similarly treated particles aggregate. To resolve this apparent contradiction, we analyze conditions necessary to hold aggregates together with electrostatic forces. We consider two different approaches: we study the effects of charge heterogeneity and particle polarization.

To study the effects of charge heterogeneity, we consider that the particle charge is described by a point charge whose locations depend on the charge distribution of the particle. Due to experimental difficulties, the location of the point charge is unaccessible thus, all possible positions for the point charge were studied with an implementation of the Metropolis algorithm. We find that charge heterogeneity can significantly alter the mechanical equilibrium of the aggregates. Another relevant parameter is the geometry of the aggregate. We find that a compact aggregate is more likely be in mechanical equilibrium.

For the study of particle polarization, we compute the forces acting on the particles by numerically solving Poisson equation. Solutions of the Poisson equation were computed using a commercially available implementation of the finite element method. We find that with the appropriate conditions the force due to particle polarization can overcome Coulomb repulsion thus, aggregates of particles charged with the same sign can be held together due to dielectric polarization. We show that a circular aggregate of identical particles can be held together due to the polarization induced by a central charge. As the size of the aggregate increases, the value of the central charge needs to increase due to the decay with distance of the electrostatic interaction.

The results presented improve the understanding of the formation of aggregates of charged particles thus, they contribute to the improvement of manufacturing efficiency as well to the understanding of the formation of planets on planetary systems, including the Earth.

Keywords — granular matter, aggregation, electrostatics, Metropolis algorithm, finite element method.

Resumo

A agregação de grãos em processos industriais e naturais está associada às interações electroestáticas. Na indústria, a agregação pode levar a graves problemas como a produção de fármacos cujos ingredientes ativos não se encontram nas concentrações corretas, em casos extremos pode ocorrer desvios de 100% nas concentrações de ingredientes chave. Também é possível que camadas de polímeros em camas vibratórias se agreguem, obrigando o encerramento temporário de fábricas para limpeza das máquinas. Na natureza, a interação electroestática pode ajudar a resolver o problema da formação de planetesimais com tamanhos da ordem do milímetro. O problema da formação de planetesimais surge porque a grandes escalas, da ordem do quilómetro, o crescimento dos corpos é promovido pela atração gravita. Porém, a escalas mais pequenas as forças gravíticas não são fortes o suficiente para manter os corpos em contacto durante as colisões, o rácio entre a forca gravítica e as forças durante as colisões cresce linearmente com o tamanho dos corpos. Para escalas mais pequenas, da ordem do micrómetro, o crescimento dos planetesimais é promovido pelas forças de contacto. Considerando o modelo JKR para as forças de contacto, determina-se que o rácio entre as forças de contacto e as forças durante as colisões cresce com o inverso do quadrado do tamanho dos corpos, porém existe também um tamanho a partir do qual as forças de contacto deixam de ser fortes o suficiente para promover o crescimento dos planetesimais. Como tal, a agregação de corpos de tamanho intermédio tem de acontecer devido a outra interação. A interação eletromagnética é uma possibilidade.

A forma mais simplificada da interação electroestática diz que cargas iguais se repelem, mas uma experiência, do grupo de Gerhard Wurm da universidade de Duisburg-Essen, que tenta replicar o processo de agregação de partículas carregadas num ambiente de microgravidade mostra que é possível existirem agregados cujas partículas têm maioritariamente cargas com o mesmo sinal. A condições que permitem partículas idênticas atrair não são óbvias. Neste trabalho analisamos quais as condições necessárias para estabilizar agregados através de forças electroestáticas. Uma vez que estamos a lidar com partículas isolantes iremos ter em conta duas propriedades: a obtenção de carga devido ao efeito triboelétrico e a polarização de partículas na presença de um campo elétrico.

O efeito triboelétrico, ainda não totalmente compreendido, permite a obtenção de cargas em materiais isolantes. A forma mais conhecida deste fenómeno é observada quando se esfrega um balão no nosso cabelo, carregando o balão de borracha. O efeito triboelétrico é o processo de troca de cargas na área em redor do ponto de contacto entre duas partículas isolantes em colisão, como tal a carga total de cada partícula aumenta. Uma vez que este efeito é local, após múltiplas colisões a superfície de cada partícula tem a carga distribuída de forma heterogénea. Para refletir essa heterogeneidade, consideramos que a carga de cada partícula é bem aproximada por uma carga (pontual) virtual cuja localização reflete a distribuição de carga da partícula. A interação entre cargas é calculada através da lei de Coulomb. Atualmente, é impossível medir experimentalmente, de forma precisa, a distribuição de cargas de uma partícula pelo que é impossível saber onde colocar a carga virtual. O equilíbrio mecânico de agregados de partículas esféricas foi avaliado através da implementação de um algoritmo de Metropolis que percorre o

espaço de configurações possíveis para os centros de carga. A convergência do algoritmo é medida tendo por base o quão longe o agregado se encontra do equilíbrio mecânico. O equilíbrio mecânico de um agregado é obtido quando a força que atua na carga virtual de uma partícula aponta para uma partícula vizinha, de forma a maximizar o atrito (proporcional à força normal em relação ao ponto de contacto) entre partículas. Também se considera que uma partícula está em equilíbrio em relação às outras do agregado quando a força que atua na carga virtual aponta para um espaço cujo tamanho é mais pequeno que o diâmetro da partícula, uma vez que se assume que as forças envolvidas não são suficientes para deformar as partículas.

Foi possível mostrar que o equilíbrio mecânico dos agregados pode resultar da heterogeneidade na distribuição de carga. Em particular, um agregado formado por três partículas cuja carga é distribuída de forma heterogénea na superfície apresenta um número de combinações de carga que permitem equilíbrio mecânico significativamente maior quando comparado com o mesmo agregado de partículas cujas cargas estão distribuídas de forma homogénea. Para este agregado foi também determinada uma expressão analítica que permite avaliar o equilíbrio mecânico. Por fim, foi estudado o efeito da geometria do agregado no equilíbrio mecânico. Através de uma análise estatística de agregados com carga escolhida aleatoriamente segundo uma gaussiana mostra-se que quanto mais compacto for o agregado, maior é a probabilidade de ele estar em equilíbrio mecânico. Confirmou-se também que agregados com carga total próxima de zero têm maior probabilidade de equilíbrio mecânico, isto porque há maior equilíbrio entre as forças atrativas e repulsivas.

Na presença de um campo elétrico materiais isoladores polarizam. Essa polarização altera o campo elétrico em redor das partículas isoladores e pode inclusive ser responsável pelo deslocamento induzido por forças electroestáticas de partículas neutras. Soluções analíticas da equação de Poisson com partículas dielétricas mostram que as forças devido à polarização dependem da distância entre partículas carregadas da mesma maneira que a lei de Coulomb, que depende do inverso do quadrado da distância. Dada a dificuldade em obter soluções analíticas, para os casos de interesse nesta tese, resolveu-se numericamente numericamente a equação de Poisson. As soluções foram obtidas usando o método dos elementos finitas implementado pelo software COMSOL Multiphysics®.

Quando a polarização é considerada, e quando as condições são apropriadas, é possível que duas partículas cuja carga apresenta o mesmo sinal se atraiam. Isto acontece quando a atração devido à polarização das partículas é maior do que a repulsão de Coulomb devido às cargas das partículas. Por outro lado, também é possível obter repulsão entre duas partículas de cargas opostas. Para este caso, a constante dielétrica, relacionada com a polarização, tem de ser tal que é o meio envolvente, e não as partículas, que polariza. Esta polarização, presente no meio envolvente em torno das partículas, funciona como um escudo para a atração de Coulomb. Considerando agregados com simetria circular compostos por partículas com o mesmo raio e carga, determinou-se qual a magnitude necessária para que uma carga central estabilize o agregado. O estudo da magnitude da carga central foi feito para agregados de vários tamanhos. Para estes agregados, mostra-se que a carga central pode estabilizar agregados compostos todos pela mesma carga, porém a magnitude da carga central tem de aumentar com o tamanho do agregado. Só assim é possível que as partículas na orla exterior do agregado sejam polarizadas o suficiente de maneira a que a atração devido à polarização se sobreponha à repulsão devido à interação de Coulomb.

Em suma, ao longo do texto é mostrado como distribuições heterógenas de carga podem promover a agregação de partículas carregas. Mostra-se também que esse comportamento pode ser amplificado devido à polarização das partículas. A polarização pode inclusive promover a agregação de partículas com o mesmo sinal de carga. Os resultados desenvolvidos ao longo da tese permitem melhorar a com-

preensão dos processos de agregação de partículas carregadas contribuindo para evitar complicações em processos industriais e para a compreensão da formação de planetas em sistemas planetários, incluindo o planeta Terra.

Palavras chave — matéria granular, agregação, electroestática, algoritmo de Metropolis, método dos elementos finitos.

Contents

List of Figures

List of Tables

Chapter 1

Introduction

Electrostatic attraction is central to both industrial and natural aggregation processes. Industrially, this leads to profound problems, for example producing variations, by as much as 100%, in active ingredient concentrations in common pharmaceuticals [1]. Likewise sticking of thick layers of polymers to fluidized bed risers [2,3] forces manufacturing shut-downs to scour the risers. Particle aggregation also contributes to material inhomogeneities that produce a documented 50% rejection rate in manufactured ceramics [4].

In nature, electrostatics can provide the necessary attraction for planets formation to occur. In protoplanetary disks, planets emerge from the aggregation of dust (micrometer) particles, like chondrites, into large-scale structures, like asteroids, see figure 1.1. For large aggregates, it is well known that the main attractive interactions are gravitational [5]. The aggregation even increases with the size (radius) of the aggregates since the ratio between gravity and the forces involved on the collisions grow linearly with the size of the aggregate R. In the size range below about 10 μm, particles can stick due to sticking forces [6]. Using the Johnson-Kendall-Roberts (JKR) or Derjaguin-Muller-Toporov (DMT) model, that consider the stored elastic energy and the lost surface energy in a solid [7, 8], the ratio between sticking forces and the forces during collisions is proportional to R^{-2}. In between these two regimes there is a size range for which it is not clear what are the relevant attractive forces, for sticking and gravitational forces are not strong enough to justify the observed structures [9–11].

An experimental work performed by the group of Professor Gerhard Wurm at the University of Duisburg-Essen [12, 13], shows that electrostatic interactions may be responsible for intermediate aggregate sizes. On the laboratory, millimeter-sized charged glass beads are released into a micro gravity environment with the presence of a constant electric field, where it is possible to observe charged grain aggregates moving under the influence of the electric field. Analytic calculations [14, 15], and numerical simulations [16–18] also provide evidence that aggregates can be stabilized by electrostatic interactions. In particular, Singh and Mazza [19] have used particle-based simulations to evolve a system of several spherical particles, with random initial position and velocity, which interact via electrostatic forces. They observed the formation and growth of particle aggregates.

Although we are dealing with insulators, charge is present due to tribocharging. This phenomenon is characterized by the buildup of charges upon the collision of insulators and can significantly alter the dynamics of granular systems. The mechanism behind tribocharging is still under debate. However, experiments by several groups have shown that grains mutually charge upon collision and that the charge differences even increase with multiple collisions. Yoshimatsu et al. have shown that such transfer of charge might result in an exponential growth of the electromagnetic field in a particle bed [20].

The problem of determining what charges promote aggregation is yet to be solved. Like charged grains should repel, and so electrostatic attraction requires charge heterogeneity. It is currently unclear

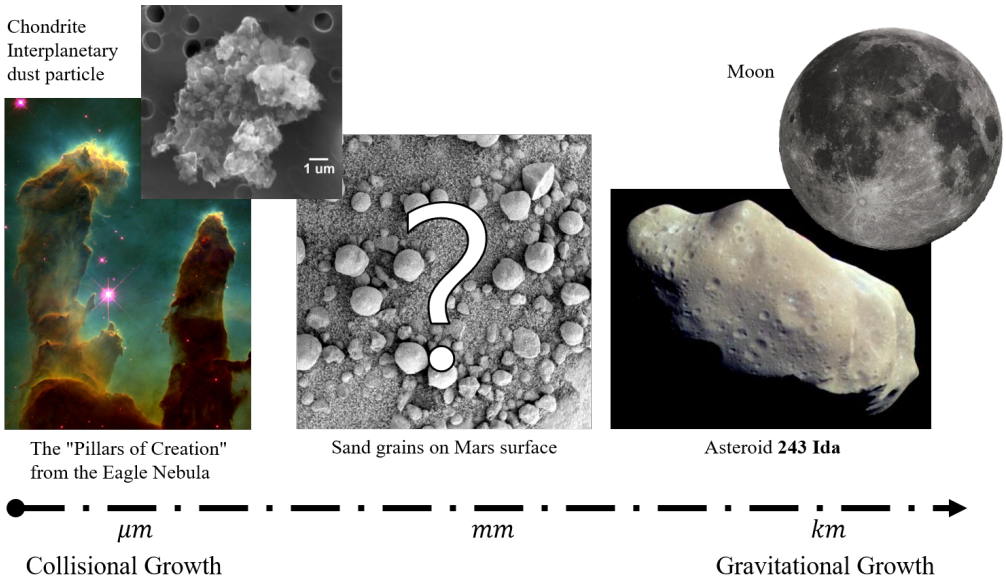

Figure 1.1: Three stages of planet formation. From left to right, the aggregation of micrometer dust particles due to sticking forces, the mechanism behind aggregation of millimeter particles is still unknown and kilometer particles aggregate into planets via gravitational attraction.

how grains acquire sufficiently dissimilar charges to avoid Coulomb repulsion, and how dissimilar these charges must be to account for the formation of multiparticle aggregates.

Recent computations by Feng [17] provide insight into this problem by demonstrating that two dielectric particles with identical sign charges can attract if the magnitude of charges on the particles differ significantly, and the particle permittivity is sufficiently high. The mechanism explored in Ref. [17] is that induced dipole-dipole attraction can overcome Coulomb repulsion if the former is large and the latter is small.

In this work, we aim at identifying under which conditions are the electrostatic interactions able to mechanically stabilize the aggregates. We will focus on the numerical study of two key grain properties, the heterogeneous charge distribution due to collisional charging and grain polarization in the presence of an electric field.

Chapter 2

Electrostatics of dielectric particles

Finding the electric potential V induced by a certain distribution of charges ρ is a boundary value problem. The differential equation to be solved is the Poisson equation

$$\nabla^2 V(\vec{x}) = -\frac{\rho(\vec{x})}{\varepsilon_0}, \tag{2.1}$$

where ε_0 is a constant denominated the vacuum permittivity. The electrostatic potential relates to the electric field $\vec{E}$ by

$$\vec{E} = -\nabla V. \tag{2.2}$$

Combining Eq. (2.1) and (2.2) we obtain Gauss law of electrostatics

$$\nabla \cdot \vec{E}(\vec{x}) = -\frac{\rho(\vec{x})}{\varepsilon_0}. \tag{2.3}$$

A simple problem is the determination of the electric field induced by a sphere of radius R and charge Q. Let us calculate the electric field on the surface of a sphere with the same center as the previous one and with radius $r > R$ by integrating the Gauss law over Ω, the volume of the sphere with radius r,

$$\iiint_\Omega \nabla \cdot \vec{E}(\vec{x}) dV = \iiint_\Omega \frac{\rho(\vec{x})}{\varepsilon_0} dV. \tag{2.4}$$

Because only exists charge inside the sphere with radius R we know that the integral on the right-hand side equals the total charge Q. The integral on the left-hand side can be simplified using Gauss law. Thus

$$\iint_{\partial\Omega} \vec{E}(\vec{x}) \cdot \vec{n} dA = \frac{Q}{\varepsilon_0}. \tag{2.5}$$

Due to the symmetry of the problem, we know that the electric field only has a radial component thus, we can determine that the integral on the left-hand side is $4\pi r^2 \vec{E}(r)\vec{e}_r$. And so, we recover Coulomb's law

$$\vec{E}(r) = k_e \frac{Q}{r^2} \vec{e}_r, \tag{2.6}$$

where $k_e = 1/(4\pi\varepsilon_0)$ is Coulomb's constant and $\vec{e}_r$ is the unitary vector that points away from the center of the sphere. The force acting on a charge q at position $\vec{r}$ due to the electric field $\vec{E}$ is simply

$$\vec{F} = q\vec{E}(\vec{r}). \tag{2.7}$$

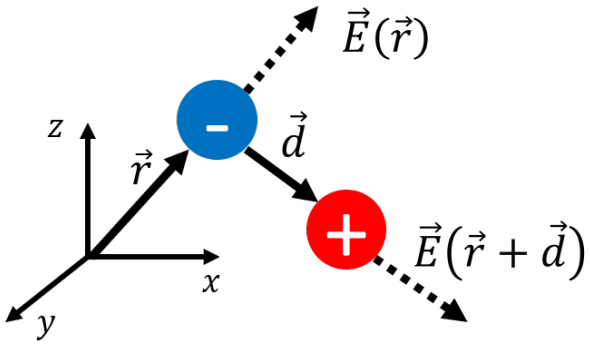

Figure 2.1: Scheme of a dipole composed of two charges Q separated by $\vec{d}$. The position of the negative charge is $\vec{r}$ and so the position of the positive one is $\vec{r}+\vec{d}$. The dipole is under the electric field $\vec{E}$.

When we are dealing with particles with volume, we need to integrate the infinitesimal version of Eq. (2.7) over the volume of the particle Ω to determine the total force acting on the particle

$$\vec{F} = \iiint_{\Omega} \rho \vec{E} dV. \tag{2.8}$$

Combining this equation with Eq. (2.3) we obtain that the force that acts on a particle is given by the integral of Maxwell stress tensor [21] over the surface $\partial\Omega$, *i.e.*

$$\vec{F} = \iint_{\partial\Omega} \varepsilon_0 \left[\vec{E} \otimes \vec{E} - \frac{1}{2} \left(\vec{E} \cdot \vec{E} \right) \mathbf{I} \right] \vec{n} dS, \tag{2.9}$$

where $\otimes$ is the dyadic product, $\mathbf{I}$ is the identity matrix and $\vec{n}$ is the unitary vector normal to the particle surface.

Using Coulomb's law, it is possible to determine that the field due to a dipole, *i.e.* two charges of equal magnitude and opposite sign separated by $\vec{d}$, as represented in Fig. 2.1, is

$$\vec{E}(\vec{x}) = k_e \frac{3\left(\vec{p}\cdot\hat{x}\right)\hat{x} - \vec{p}}{\|\vec{x}\|^3}, \tag{2.10}$$

where $\vec{p} = Q\vec{d}$ is the dipole moment [22]. The dipole is the second term of the multipole expansion, used to determine the electric field of arbitrary charge distributions. The description of the electric field by the multipole expansion is based on principal of superposition, that Poisson equation obeys, and can be thought as the sum of the electric fields due to several point charges. The number of point charges depends on the desired accuracy.

Let us now consider the position of the negative charge to be $\vec{r}$ and the position of the positive one to be $\vec{r}+\vec{d}$, as represented in figure 2.1. The force acting on a dipole is

$$\vec{F} = Q\vec{E}(\vec{r}+\vec{d}) - Q\vec{E}(\vec{r}). \tag{2.11}$$

By considering the x component of the force and expanding the first term we have

$$\begin{aligned} F_x &= Q\left[E_x(x+d_x, y+d_y, z+d_z) - E_x(x,y,z)\right] = \\ &= Q\left[E_x(x,y,z) + d_x\frac{E_x}{\partial x} + d_y\frac{E_x}{\partial y} + d_z\frac{E_x}{\partial z} - E_x(x,y,z)\right]. \end{aligned} \tag{2.12}$$

The first and last terms cancel out. This equation in conjunction with the equivalent ones for F_y and F_z can be simplified and we obtain that the force acting on a dipole with moment $\vec{p}$ due to the electric field $\vec{E}(\vec{r})$ is

$$\vec{F} = \vec{p} \cdot \nabla \vec{E}. \tag{2.13}$$

Going back to Poisson equation, when there is charge accumulated on a surface, for example on the surface of a sphere with radius R, the Poisson equation is different. Because only exists charge at the surface of the sphere we have

$$\rho(\vec{x}) = \sigma(\vec{x})\delta(r - R), \tag{2.14}$$

where σ is the surface charge density. Thus

$$\iint_{\partial\Omega} \vec{E}(\vec{x}) \cdot \vec{n} dA = \iiint_{\Omega} \frac{\sigma(\vec{x})\delta(r-R)}{\varepsilon_0} dV = \iint_{\partial\Omega} \frac{\sigma(\vec{x})}{\varepsilon_0} dA. \tag{2.15}$$

Because the first term can be interpreted as the electric flux through the sphere surface, we can simplify the equation

$$\left[\vec{E}_{\text{out}}(\vec{x}) - \vec{E}_{\text{in}}(\vec{x})\right] \cdot \vec{n} = \frac{\sigma(\vec{x})}{\varepsilon_0}. \tag{2.16}$$

And so, we obtain that on a charged surface there is a discontinuity on the electric field of $\sigma(\vec{x})/\varepsilon_0$.

2.1 Dielectric materials

Under an electric field, the collective displacement of the electronic clouds results in polarized dielectrics. On linear dielectrics the polarization density $\vec{P}$ is proportional to the electric field $\vec{E}$ by a constant named polarizability χ_e

$$\vec{P} = \varepsilon_0 \chi_e \vec{E}. \tag{2.17}$$

It is possible to show, see Ref. [21], that the polarization is related to a charge density, usually named bound charge density ρ_b, by

$$\rho_b = -\nabla \cdot \vec{P}. \tag{2.18}$$

Thus, on a dielectric the total charge density is

$$\rho = \rho_f + \rho_b, \tag{2.19}$$

where ρ_f is the density of free charge, *i.e.* all the charges present that are independent of the electric field. Combining Eq. (2.3), (2.18) and (2.19) results in

$$\nabla \cdot \left[(1 + \chi_e)\, \vec{E}\right] = \frac{\rho_f}{\varepsilon_0}. \tag{2.20}$$

The expression inside the regular brackets can be interpreted as the relative permittivity thus beeing equivalent to the Gauss law in the presence of dielectrics

$$\nabla \cdot \left[\kappa \vec{E}\right] = \frac{\rho_f}{\varepsilon_0}, \tag{2.21}$$

where $\kappa = (1 + \chi_e)$ is the relative permittivity, or dielectric constant, and it may depend on the position. Notice that, because a dielectric constant is present Eq. (2.16) becomes

$$\left[\kappa_{\text{out}}\vec{E}_{\text{out}}(\vec{x}) - \kappa_{\text{in}}\vec{E}_{\text{in}}(\vec{x})\right] \cdot \vec{n} = \frac{\sigma(\vec{x})}{\varepsilon_0}. \tag{2.22}$$

Manipulating Eq. (2.21) results in

$$\kappa \nabla \cdot \vec{E} = \frac{\rho_f}{\varepsilon_0} - (\nabla\kappa) \cdot \vec{E}. \tag{2.23}$$

For a system with constant permittivity the last term is zero and so the bound charges, related to κ, only change the magnitude of the field. When $\kappa \equiv \kappa(\vec{x})$ bound charges arise that alter the electric field, and consequently the forces.

2.1.1 Dielectrophoretic force

Let us consider a dielectric sphere with radius R and dielectric constant κ. Acting on the sphere is a constant electric field $\vec{E}_0 = E_0\vec{e}_z$. We will determine the changes to the electric field due to sphere polarization. There are no net charges in the system and we are dealing with spheres thus, we will use a solution to the Laplace equation (Poisson equation for the particular case of $\rho = 0$) [22]. The solution for a field with spherical and axial symmetry is

$$V(r, \theta) = \sum_{n=0}^{\infty} \left(A_n r^n + B_n r^{-(n+1)}\right) P_n(\cos\theta), \tag{2.24}$$

where the origin of the coordinates in on the center of the sphere with radius R, A_n and B_n are constants to be determined and $P_n(\cos\theta)$ is the Legendre polynomial of order n. We will split the problem in to the determination of the potential inside the sphere $V^{(i)}$ and on the outside $V^{(e)}$. Inside the sphere all constants $B_n^{(i)}$ are zero because we cannot have an infinite potential for $r = 0$. So

$$V^{(i)} = \sum_{n=0}^{\infty} A_n^{(i)} r^n P_n(\cos\theta). \tag{2.25}$$

On the outside, we have that for $r \gg R$ the field remains unaffected. Because of Eq. (2.2) we can determine that

$$V(r \gg R, \theta) = -E_0 z = -E_0 r\cos\theta. \tag{2.26}$$

Since $P_1(\cos\theta) = \cos\theta$, we conclude that $A_1^{(e)} = -E_0$ and $A_n^{(e)} = 0$ for $n \neq 1$ thus,

$$V^{(e)} = -E_0 r\cos\theta + \sum_{n=0}^{\infty} B_n^{(e)} r^{-(n+1)} P_n(\cos\theta). \tag{2.27}$$

To determine the remainder constants, we need to impose that on the boundary of the sphere the potential is continuous and that Eq. (2.22) holds,

$$\begin{aligned} V^{(i)}(R, \theta) &= V^{(e)}(R, \theta), \\ \kappa\nabla V^{(i)}(r, \theta)\Big|_{R,\theta} &= \nabla V^{(e)}(r, \theta)\Big|_{R,\theta}. \end{aligned} \tag{2.28}$$

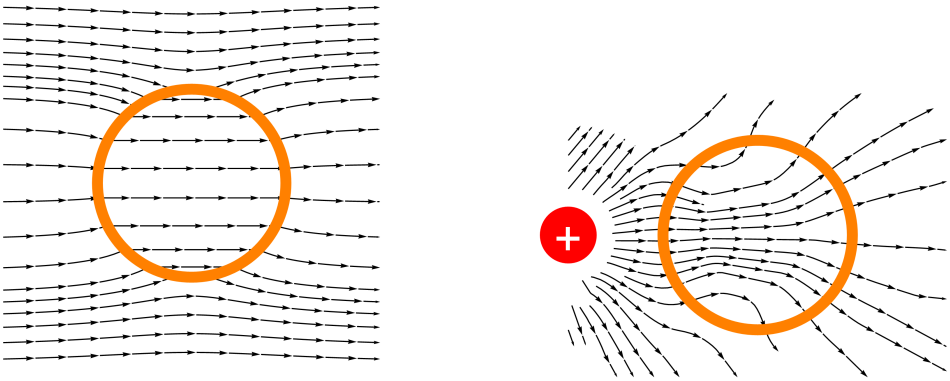

(a) (b)

Figure 2.2: Projection on the xz plane of the electric field lines of $\vec{E} = E_0\vec{e}_z$, on the left, and of a positive point charge, on the right, in the presence of a dielectric sphere. The orange circle represents the surface of the sphere.

Using the above conditions results in

$$\begin{aligned} B_n^{(e)} &= A_n^{(i)} = 0 \qquad \text{for } n \neq 1, \\ A_1^{(i)} &= -\frac{3E_0}{2+\kappa}, \\ B_1^{(e)} &= \frac{\kappa-1}{\kappa+2}E_0R^3. \end{aligned} \tag{2.29}$$

We can now write the final expressions for the potential

$$\begin{aligned} V^{(i)}(r,\theta) &= -\frac{3E_0}{\kappa+2}r\cos\theta && r \leq R, \\ V^{(e)}(r,\theta) &= -E_0 r\cos\theta + \frac{\kappa-1}{\kappa+2}\frac{R^3E_0\cos\theta}{r^2} && r \geq R. \end{aligned} \tag{2.30}$$

and, using Eq. (2.2), the expression of the electric field

$$\begin{aligned} \vec{E}^{(i)}(r,\theta) &= \frac{3}{\kappa+2}\vec{E}_0 && r \leq R, \\ \vec{E}^{(e)}(r,\theta) &= E_0\cos\theta\left(1+\frac{\kappa-1}{\kappa+2}\frac{2R^3}{r^3}\right)\vec{e}_r + E_0\sin\theta\left(-1+\frac{\kappa-1}{\kappa+2}\frac{2R^3}{r^3}\right)\vec{e}_\theta && r \geq R. \end{aligned} \tag{2.31}$$

Notice that inside the sphere the field is the same as the original field but attenuated. The electric field lines are represented in Fig. 2.2a.

Since the electric field is constant inside the sphere, using Eq. (2.17) the polarization of the sphere is

$$\vec{p} = \frac{4}{3}\pi R^3\vec{P} = \frac{4}{3}\pi R^3\varepsilon_0(\kappa-1)\vec{E}^{(i)} = 4\pi R^3\varepsilon_0\frac{\kappa-1}{\kappa+2}\vec{E}_0. \tag{2.32}$$

Thus, using Eq. (2.13) we can determine the force acting on the sphere. But, because inside the sphere the electric field is constant the net force is zero. This can be interpreted as the pull due to the electric field on the left of the particle is the same as the one on the right, thus the forces add up to zero.

When the electric field is not constant the polarized sphere can move under an electric field, even if it has zero charge. For example, a dielectric sphere has a large impact on the electric field due to a point charge, see figure 2.2b. For this case, the force acting on a neutral particle is non-zero. This is

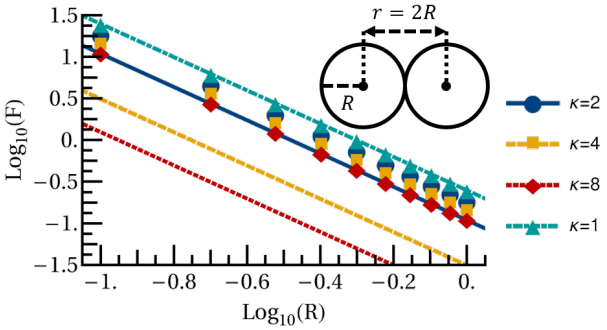

Figure 2.3: In logarithmic scale, the force between two touching identical spheres (same radius and unitary charge), in units of k_e, as function of the particle radius R for different dielectric constants κ, represented with different colors. The lines represent the values obtained by equation (2.34) and the points represent the force obtained by solving Poisson's equation.

because near the point charge the polarization is larger than the polarization on the opposite side of the sphere thus, there is an asymmetry on the forces. It can be calculated that the force due to polarization, the dielectrophoretic force, induced by a point charge is given by [23]

$$F_{DEP} = \frac{Q^2}{4\pi\varepsilon_0}\sum_{j=1}^{\infty}\frac{R^{2j+1}}{r^{2j+3}}\frac{j(j+1)(\kappa-1)}{j(\kappa+1)+1}, \tag{2.33}$$

where r is the distance between the sphere center and the point charge and Q is the magnitude of the point charge. If we have two uniformly charged dielectric spheres with the same radius R in contact, we can approximate the forces acting on the spheres by the sum of the Coulomb interaction and the dielectrophoretic force. Because the distance between the centers of the spheres is related to the radius by $r = 2R$ the above expression can be simplified

$$F_{DEP} = \frac{Q^2}{4\pi\varepsilon_m}\frac{1}{R^2}\sum_{j=1}^{\infty}\frac{1}{2^{2j+3}}\frac{j(j+1)(\kappa-1)}{j(\kappa+1)+1} \tag{2.34}$$

thus, the dielectrophoretic force has the same dependence on the particle radius as Coulomb interaction, see Eq. (2.6) and (2.7).

In Fig. 2.3 is the comparison between the force calculated using Eq. (2.7) and (2.34) (lines) and the force calculated by numerically solving Poisson's equation (points) for different values of dielectric constant, κ. The method to obtain the numerical solution is discussed in chapter 4. When there is no polarization $\kappa = 1$ the values predicted by Eq. (2.7) agree with the values obtained by solving Poisson. The same is not true when polarization is present $\kappa = \{2, 4, 8\}$ thus, showing that the approximation of the dielectrophoretic force due to a point charge is not good enough. Nevertheless, the force obtained by solving Poisson has the same dependence on the particle radius as the Coulomb interaction. A less simple expression for the dielectrophoretic force between two spheres is derived by Ref. [14], the force between two charged dielectric spheres is given by

$$\begin{aligned} F = &\frac{\kappa+2}{\kappa-1}\frac{1}{R}a_1 + \\ &+\frac{4\pi\varepsilon_0}{\kappa-1}\sum_{n=1}^{\infty}\big[(n+1)(\kappa+1)+1\big]a_n a_{n+1}, \end{aligned} \tag{2.35}$$

where a_i represents an infinite sum that is linear with respect to Q. The infinite sum appears because of the non-linear interaction between polarized spheres. Thus, the electrostatic force F acting on a particle

relates to the charge of the second particle according to a second order polynomial [24]

$$F(Q) = \alpha Q^2 - \beta Q + \gamma, \tag{2.36}$$

where the constant β define the Coulomb interaction (first term in Eq. (2.35)), and the constants α and γ define the force due to particle polarization.

2.2 Final remarks

Problems involving charged particles are solved using the Poisson equation. At first order approximation, the interaction between two particles is calculated using Coulomb law. For dielectric matter the first order approximation is not enough, and neutral particles are sensitive to an electric field. The force due to polarization has the same dependence on the distance as Coulomb law and the interaction between two dielectric spheres can be described by a second order polynomial.

Chapter 3

Heterogeneous charge distribution

There are no free-charge carriers on the surface of a grain, so tribocharging results in a heterogeneous charge distribution on the surface of the grains. As time evolves, multiple collision between grains occur and so, each grain has multiple regions where charge exchange happened resulting in a grain whose surface is heterogeneously charged. Due to poor electric conductivity the grains remain heterogeneously charged for long periods of time.

The contribution to the electrostatic force from each charge q_i is given by the summing Eq. (2.6) over all other charges

$$\vec{F}_i = -k_e q_i \sum_{j \neq i} q_j \frac{\vec{e}_{ij}}{r_{ij}^2}, \tag{3.1}$$

where r_{ij} is the distance between charge i and j and $\vec{e}_{ij}$ is the unitary vector that goes from charge i to j. When working with arbitrary charge distributions, it is standard procedure to use the multipole expansion [21, 22]. The traditional implementation of the multipole expansion in problems of charged granular matter is to consider the center of the multipole expansion to coincide with the geometrical center of the grain. However, this does not always provide the most accurate description. In fact, by finding the optimal location for the charges, we can improve the precision of the approximation for the same order of the multipole expansion [25].

The heterogeneous charge distribution on the grains can affect significantly the forces acting on the grains. For example, in a uniform electric field, the force acting on a uniform charged spherical grain can be calculated by considering that all its charge is concentrated in the geometrical center of the grain. When the charge is not distributed in a symmetric and uniform way, the force calculation is not so simple. We will describe the charge of the grain with a virtual (point) charge optimally placed inside the grain but not necessarily on the center and consider only monopole terms. The position of the charge inside the grain will be determined following an optimization procedure discussed below. The interaction between grains is given by Eq. (3.1) where the sum is over all charges. Because in this case the virtual charge is not necessarily in the center of the grain, even in a uniform electric field, the grain can perform both translational and rotational motion.

On the contact point between two grains there is Coulomb friction that opposes the relative (rotational) motion of the grains. We assume that this force $\vec{F}_T$ is given by Coulomb's law of friction [24, 26] that states that:

- The force does not depend on the area of contact between grains;
- The force $\vec{F}_T$ opposes the force that induces movement and is proportional to the force normal to

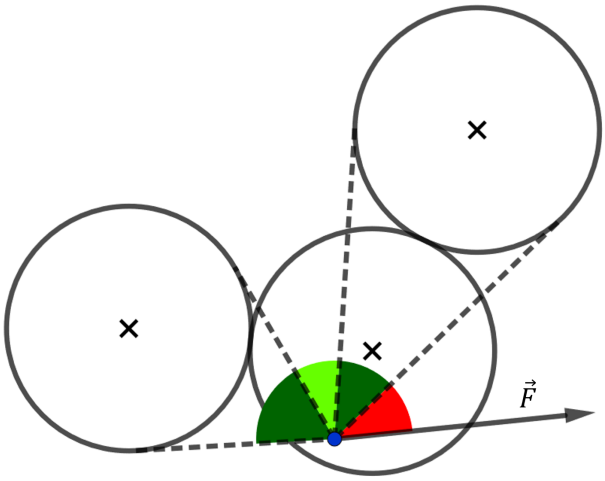

Figure 3.1: Schematic representation of the directions allowed, angles in green, for the force acting on the virtual charge, blue dot. The dark green angles represent the directions pointing to a neighboring grain, the light green angle is a region, in between two neighbors that is too small for movement to occur in that direction without grain deformation. The red angle quantifies how much is the force from the green region.

the point of contact

$$|\vec{F}_T| = \mu |\vec{F}_n|; \tag{3.2}$$

- The friction coefficient μ depends on the material of the grain.

Because the friction coefficient is material specific, we investigate the equilibrium of the aggregates by maximizing $|\vec{F}_n|$, thus maximizing the odds of the grains remaining stationary in relation to each other. We will assume that if the force acting on the virtual charge points towards a neighboring grain, see dark green angle in Fig. 3.1, the grains will not move relative to each other.

For simplicity, we neglect also forces related to grain deformation. Usually these forces are non-linear with respect to the deformation, but a possible approximation is to consider the grains are elastic solids. With this approximation it is possible to conclude that the collision timescale is very small $\sim 10^{-6}$s [24, 27] result of strong forces that oppose deformation[1]. Thus, we will assume that the forces acting on the grains are not strong enough to deform them. Thus, if the force acting on a grain points towards a gap in between two neighbors that is smaller than the grain diameter, see light green angle in Fig. 3.1, the grain will maintain its position relative to its neighbors.

In summary, we assume that a grain keeps its position relative to its neighbors if the force acting on its virtual charge acts in a direction **i)** towards a neighbor, or **ii)** towards a gap in between the neighbors smaller than the grain diameter. If the force acting on all virtual charges respect one of these conditions, the aggregate is considered to be in mechanical equilibrium, *i.e.* the relative position of its grains does not change over time.

3.1 Metropolis algorithm

To evaluate the mechanical equilibrium of an aggregate composed of grains, whose charge is known but the charge distribution around each grain is not, we will use an implementation of the Metropolis

[1]Numerical work requires special care on handling collisions. Due to very small collision timescales a very small timestep is required to accurately calculate the contact dynamics in molecular dynamics simulations. For systems with several grains this is computational demanding. The solution to the problem can either be perform event driven simulations, not always possible or desirable, or to increase the timescale of the collisions by simulating "softer" grains, with smaller elastic constants.

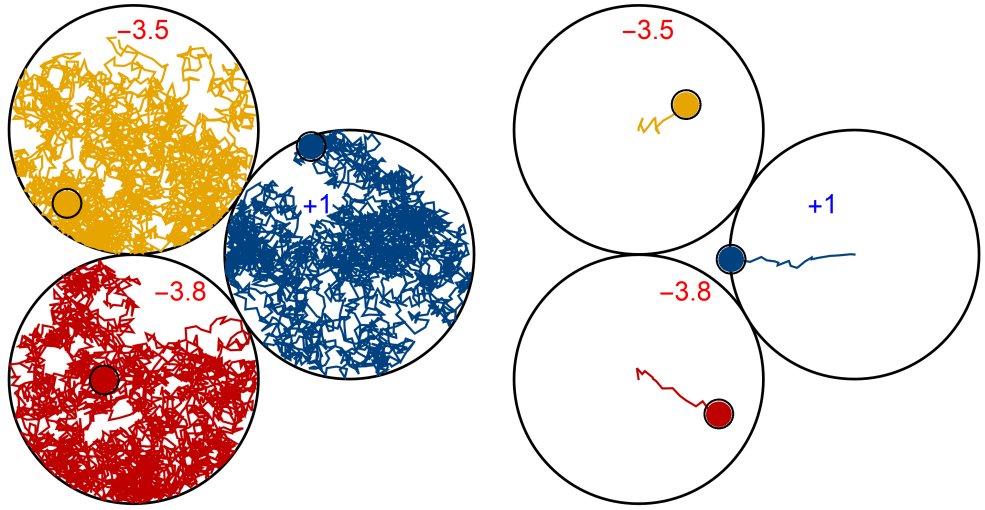

(a) $T = 10^{-1}$ (b) $T = 10^{-4}$

Figure 3.2: Examples of the trajectories of the virtual of charges during the Metropolis algorithm for two different "temperatures". Large points represent the final position of the charges and the numbers represent the charge values.

algorithm, a Markov Chain Monte Carlo method, to run over the configuration space of the virtual charges in search of a configuration that allows for it to be in mechanical equilibrium.

The implementation of Metropolis requires the definition of a probability of acceptance of a state, in our case it will be how far the aggregate is from mechanical equilibrium, measured by the red angle in Fig. 3.1. The red angle is the angle that the force acting on the virtual charge makes with the green region. When the red angle is negative the force acting on that grain respects one of the equilibrium criterion, *i.e.* it points towards a green region. Notice that two angles can be measured between the force and green region, the red angle is always the smallest of the two. In the Metropolis algorithm, we will generate new trials of the configuration of the virtual charges until it converges into a point of the configuration space where all red angles are negative. The acceptance probability of a new trial is

$$P = \exp\left(\frac{\theta_i - \theta_{i-1}}{\theta_i}\frac{1}{T}\right), \tag{3.3}$$

where θ_i is the largest red angle of trial i and T is the "temperature". This "temperature" has no physical meaning but it allows the control of the probability of accepting a state with $\theta_i > \theta_{i-1}$. Notice that if the largest red angle decreases the probability is larger than 1, as consequence when $\theta_i < \theta_{i-1}$ the new trial is always accepted then, the proper expression for the probability is

$$p = \min\left\{1, \exp\left(\frac{\theta_i - \theta_{i-1}}{\theta_i}\frac{1}{T}\right)\right\} \tag{3.4}$$

The implementation of the Metropolis algorithm is as follows:

1. Start with the virtual charges at the geometrical centers of the grains;
2. Pick a random grain and move its charge a small distance ε in a direction selected uniformly at random, provided that it does not go out of the grain;
3. Calculate the electrostatic forces using Coulomb law, Eq. (2.6);
4. Calculate the red angles. If not all red angles are negative, accept the new configuration with

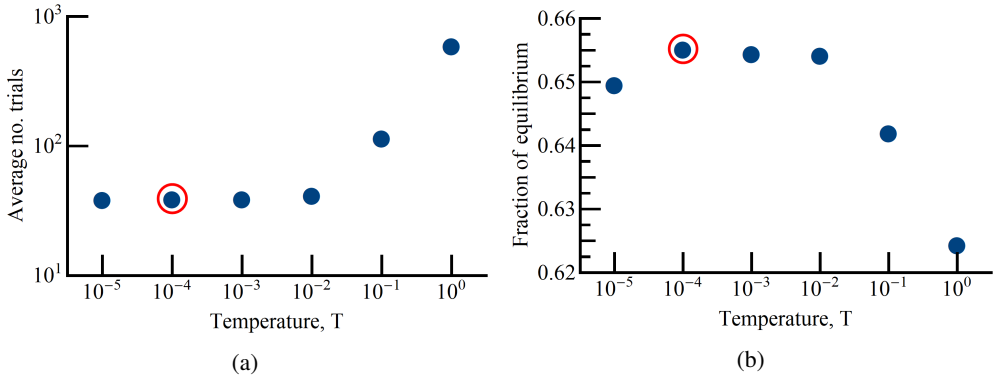

Figure 3.3: On the left, average number of trials as function of the "temperature". On the right, the fraction of aggregates with mechanical equilibrium as function of the "temperature". The points inside the red circle correspond to the "temperature" chosen.

probability p, given by Eq. (3.4). If the configuration is rejected, the charge changed in step 2 returns to its previous position;

5. Repeat 2-4 until equilibrium is found or N trials are performed.

The displacement ε of the charges is chosen randomly between zero and 10% of the grain radius.

The adjustment of the "temperature" is important to improve the convergence speed of the algorithm. For high temperatures the trajectories of the virtual charges are more erratic, as represented in Fig. 3.2a where the trajectories of the virtual charges are traced for $T = 10^{-1}$. To improve performance, *i.e.* reduce the number of trails, the "temperature" is lowered and so the virtual charges have a more direct trajectories toward the final position, as can be seen in Fig. 3.2b where the trajectories for $T = 10^{-4}$ are traced. To evaluated what is the best "temperature" the mechanical equilibrium of 10^4 aggregates were tested. The charges of the particles follow a Gaussian with mean zero and unitary standard deviation. The convergence speed was evaluated by measuring the number of trials required to find a configuration with mechanical equilibrium. Following the plot in Fig. 3.3a we see that the average number of trials required to find mechanical equilibrium increases dramatically for $T > 10^{-2}$. The fraction of aggregates with mechanical equilibrium also decreases for $T > 10^{-2}$. This happens because for high "temperature" the virtual charges change almost randomly, because most trials are accepted. Thus, the number of trials N is not enough for the system to evolve into a configuration with mechanical equilibrium. The fraction of aggregates in equilibrium also decreases for $T < 10^{-4}$. This is because for low "temperature" very few states with $\theta_i < \theta_{i-1}$ are accepted and so, the system can be stuck in a configuration where not all angles are negative and all configurations around have larger angles. Thus, we considered $T = 10^{-4}$ because it results in the best combination of speed and accuracy. To maximize the chances that all configuration with mechanical equilibrium are found without extending significantly the CPU time, we set $N = 10^4$.

3.2 Three grain aggregates

Let us first consider aggregates of two grains. Two situations are possible for these aggregates: either the charges of the grains have opposite signs or the same sign. As we are simply considering the Coulomb interaction between the virtual charges (that are equal to the total charge of the grain) when the charge of both grains has the same sign there is no location possible for the virtual charges such that the interaction is attractive. Thus, for the aggregate to be in mechanical equilibrium the charges need to have opposite

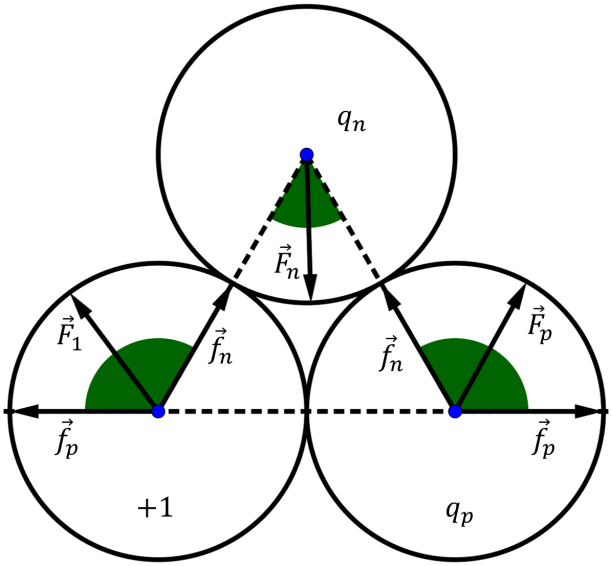

Figure 3.4: In green are the possible force directions for three grains with a unitary, a positive q_p and a negative q_n charge. The virtual charges are at the grain center. The force acting on the unitary charge is $\vec{F}_1$, on the positive one is $\vec{F}_p$ and on the negative charge is $\vec{F}_n$. The interaction with the positive and negative charges is responsible by the forces $\vec{f}_p$ and $\vec{f}_n$, respectively.

signs. Note that, if we consider the polarization of the grain, the discussion is more complicated, as explained in the next chapter.

For aggregates consisting of three charged grains there are also only two different situations for the charges, it is possible to have all three grains with the same sign charge, for example all positive, or to have two charges with the same sign and a third with a different sign, for example two positive charges and one negative. For the first case, mechanical equilibrium is never possible since no interaction between virtual charges is attractive. The second case is more interesting since there is a competition between the repulsion between the like-charge grains and the attraction between different charge grains.

Let us now analyze the mechanical equilibrium of these aggregates for the case where the virtual charges are fixed at the grain center. We will consider an aggregate composed of three grains with unitary radius and with charges Q_1, Q_2 and Q_3. Because we are interested in the case where at least one charge has different sign we consider Q_1 and Q_2 to be positive and Q_3 to be negative. Furthermore, because Coulomb law is directly proportional to the charges, see Eq. (2.6), we rescale the charges according to Q_1, and so one grain has a charge $+1$, a second one has a positive charge $q_p = Q_2/Q_1$ and the third one has a negative charge $q_n = Q_3/Q_1$.

When the three grains are in a compact configuration the forces acting on each virtual charge can be in any direction given by the green angles in Fig. 3.4. Starting with q_n, the force $\vec{F}_n$ can point between two limits, the limit where q_p is zero and so $\vec{F}_n$ points towards the charge $+1$, and the limit where $q_p \gg 1$ and so the force points towards q_p. The force acting on q_p, $\vec{F}_p$, can point between two limits, on the limit where q_n is zero $\vec{F}_p$ points away from $+1$ and on the limit where $|q_n| \gg 1$ the force points towards q_n. The limits for the charge $+1$ are similar to the ones for q_p since it is also a positive charge, and so the force $\vec{F}_1$ can point anywhere between the direction pointing towards q_n and the direction opposite to q_p.

The forces are constrained to the green region, so the force acting on q_n will always guaranty mechanical equilibrium, according to the conditions previously set. Thus, the mechanical equilibrium of the aggregate will depend on the direction of $\vec{F}_p$ and $\vec{F}_1$. We can decompose these two forces into two components, one that is pointing towards the negative charge $\vec{f}_n$ and one that points away from the positive charge $\vec{f}_p$. We will start by studying the mechanical equilibrium of the grain with charge $+1$. For it

to be in mechanical equilibrium, *i.e.* to point towards the grain with charge q_n, the horizontal component of $\vec{F}_1$ needs to be positive, thus

$$\left(\vec{f}_p + \vec{f}_n\right) \cdot \vec{e}_x \geq 0, \tag{3.5}$$

where the two force components are given by Eq. (2.6)

$$\vec{f}_p \cdot \vec{e}_x = -k_e \frac{|q_p|}{r^2} \qquad \vec{f}_n \cdot \vec{e}_x = +k_e \frac{|q_n|}{r^2} \cos(60) \tag{3.6}$$

and r is the distance between charges, which is the same for all charges. Simplifying the equations, we can obtain that the equilibrium condition is fulfilled when

$$|q_n| \geq 2|q_p|. \tag{3.7}$$

For the grain with charge q_p the force acting on it points towards the grain with charge q_n if the horizontal component of $\vec{F}_p$ is negative, thus

$$\left(\vec{f}_p + \vec{f}_n\right) \cdot \vec{e}_x \leq 0, \tag{3.8}$$

in this case the force components are

$$\vec{f}_p \cdot \vec{e}_x = +k_e \frac{|q_p|}{r^2} \qquad \vec{f}_n \cdot \vec{e}_x = -k_e \frac{|q_n||q_p|}{r^2} \cos(60) \tag{3.9}$$

and so, the mechanical equilibrium condition is

$$|q_n| \geq 2. \tag{3.10}$$

And so, since $q_n < 0$ and $q_p > 0$, if the charges obey the relations

$$q_n \leq -2 \quad \text{and} \quad q_n \leq -2q_p, \tag{3.11}$$

the aggregate can be found in mechanical equilibrium with the virtual charges located at the center of the corresponding grains. In Fig. 3.6, we represent in light blue the region of the parameter space that allows for aggregates to be in mechanical equilibrium when the virtual charge is located at the grain center.

When we move the virtual charges away from the geometrical center of the grains we alter the distance between charges. Thus, a charge combination that does not obey the conditions (3.11) can be in mechanical equilibrium, provided that the charges are correctly placed. For example, an aggregate whose charges are $+2$, $+3$ and -1 does not obey condition (3.11), but there is a position for the virtual charges that fulfills the equilibrium conditions, see figure 3.5.

We solved the problem numerically and determine the mechanical equilibrium of aggregates where one charge is fixed to Q_0 (due to the aggregate symmetry the fixed charge is arbitrary) and varied the remaining two, Q_1 and Q_2. Like for the previous case, we can rescale the charges in units of Q_0 thus obtaining $q_1 = Q_1/Q_0$ and $q_2 = Q_2/Q_0$. The results, where q_1 and q_2 were varied between 10^{-1} and 20 are in Fig. 3.6.

Starting the analysis with the first quadrant of the parameter diagram of Fig. 3.6, we see that no configuration for the position of the virtual charges was found such that all grains keep contact. This is simply because all charges are positive and so, they are all repelling each other, therefore it is impossible to have all the force vectors pointing towards another grain.

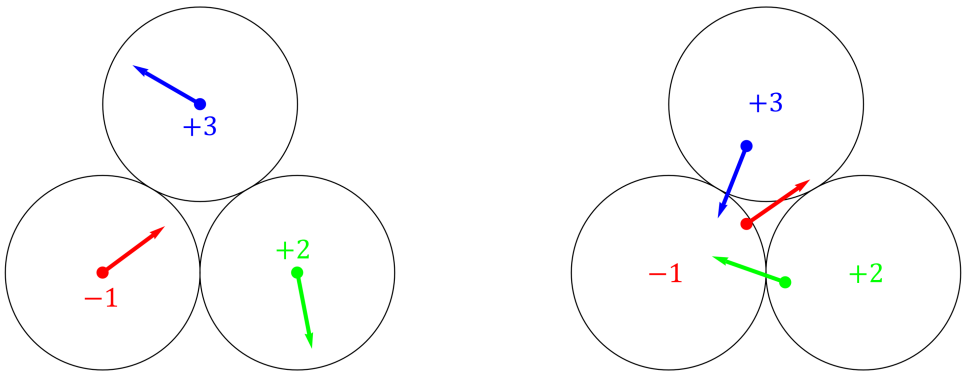

Figure 3.5: Two examples of the direction of the force vectors for a three-grain aggregate with charges $+2$ (green), $+3$ (blue) and -1 (red). On the left the virtual charges are at the geometrical center and not all vectors point to another grain, on the right the virtual charges are not on the geometrical center, but all force vectors point towards a neighboring grain.

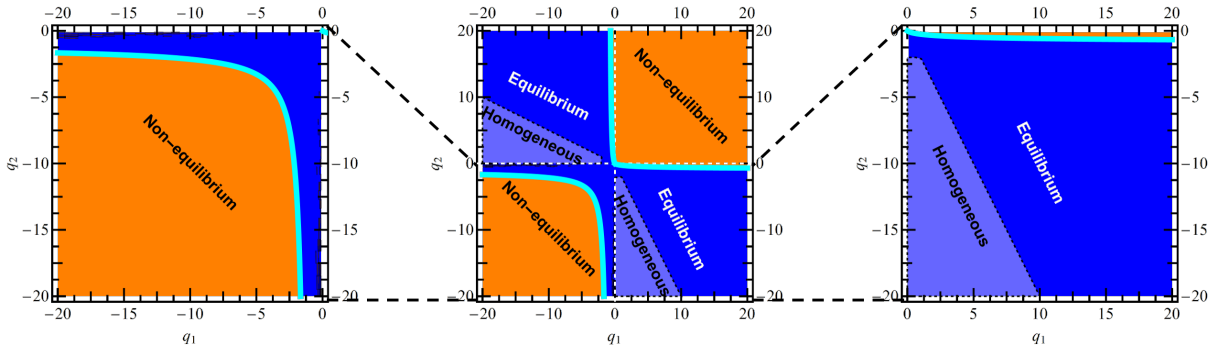

Figure 3.6: Two-parameter equilibrium diagram for a closed-packed aggregate with three grains. The charge of one grain was fixed, $Q_0 = 1$, the remaining charges were rescaled according to Q_0, q_1 and q_2, and varied between 10^{-1} and 20. Blue region (light blue for the case with the virtual charge fixed at the grain center) represents points were a configuration that keeps the grains together is found and orange regions the opposite. The cyan line corresponds to Eq. (3.15). On the sides is a zoom of the third and fourth quadrants.

Most of the aggregates in mechanical equilibrium are found on the second and forth quadrants of the plot, thus q_1 and q_2 have opposite signs. Since the plot is symmetric around the line $q_1 = q_2$, we will consider the forth quadrant, as an example, to analyze both the second and forth quadrant. In this area q_1 is positive thus for the grains to be kept together q_2 needs to be large enough to overcome the repulsion between the two positive charges. Notice that the previous condition (3.10), where q_2 corresponds to q_n is fulfilled in this quadrant. In fact, it will be shown later that if

$$q_2 < -1, \tag{3.12}$$

then a configuration for the virtual charges that balances the forces can always be found. as q_2 is strong enough to hold the remaining two charges. Recall that the same can be concluded for q_1 for the second quadrant.

In the third quadrant, both q_1 and q_2 are negative thus they are always repealing each other, and so it is Q_0 that plays the role of keeping the grains together. Given the similar situation, only one charge is responsible for holding the aggregate, a condition like Eq. (3.12) is expected. It turns out that once more, we can guaranty the equilibrium of an aggregate just by knowing the value of one varying charge,

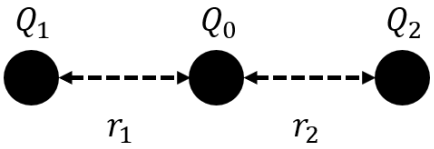

Figure 3.7: Illustration of the 1D system used to predict the boundary between equilibrium and non-equilibrium regions, cyan line in Fig. 3.6. Charge Q_1 is at a distance r_1 of charge Q_0 and r_2 separates Q_2 and Q_0.

$q_i = \{q_1, q_2\}$, because if one of the varying charges obeys the condition

$$q_i > -1, \tag{3.13}$$

it is possible for the grains to remain in contact, independently of the value of the other charge. For this case, the condition ensures that there is a balance between the magnitude of the positive unitary charge and both negative charges q_1 and q_2.

These two conditions already provide important information for understanding what charges are required to guarantee that a close-packed aggregate is in mechanical equilibrium. But as can be seen in Fig. 3.6, there are still a lot of charge combination that neither obey Eq. (3.12) nor Eq. (3.13). For example, when $q_1 = q_2 = -2$ aggregates in mechanical equilibrium are also found. In order to try to understand how it is possible for grains with charges like those to be kept in contact, a theoretical model is developed in the next section.

3.2.1 Theoretical prediction

For most equilibrium configurations obtained for different sets of charges, the virtual charges are typically placed along a line, close to each other, as seen in Fig. 3.2b. Consider three aligned charges Q_0, Q_1 and Q_2, the distance between Q_1 and Q_0 is r_1 and the distance between Q_2 and Q_0 is r_2, as represented schematically in Fig. 3.7. Since this is a 1D model, the grain represented by Q_0 cannot escape the aggregate, it is in between the two other grains. The grains on the sides, to be kept on the aggregate, need to have their net force pointing towards the central grain. That condition is easily fulfilled by imposing that the forces acting on Q_1 and Q_2 point towards the central charge,

$$F_1 = Q_1 \left(\frac{Q_0}{r_1^2} + \frac{Q_2}{(r_1 + r_2)^2} \right) > 0 \quad \text{and} \quad F_2 = Q_2 \left(\frac{Q_0}{r_2^2} + \frac{Q_1}{(r_1 + r_2)^2} \right) < 0. \tag{3.14}$$

By using the above equations and knowing that the charges, on the 2D aggregate, can be placed such that one of the two distances, r_1 or r_2, on the limit is zero, it is possible to determine that the boundary of the mechanical equilibrium for a 1D aggregate is given by

$$q_2 = -\mathrm{sgn}(q_1 + 1) \frac{q_1}{\left(1 + \mathrm{sgn}(q_1)\sqrt{|q_1|}\right)^2}, \tag{3.15}$$

where q_1 and q_2 are the rescaled charges according to Q_0 and the sign function, $\mathrm{sgn}()$, is $+1$ when the argument is positive, -1 for negative arguments and zero otherwise. This boundary is plotted in Fig. 3.6 in cyan, and it is in good agreement with the boundaries of equilibrium obtained numerically with the Metropolis algorithm. Notice that in the limit of $|q_1| \gg 1$ the aggregate is in mechanical equilibrium for $q_2 = -1$ thus, recovering Eq. (3.12) and (3.13).

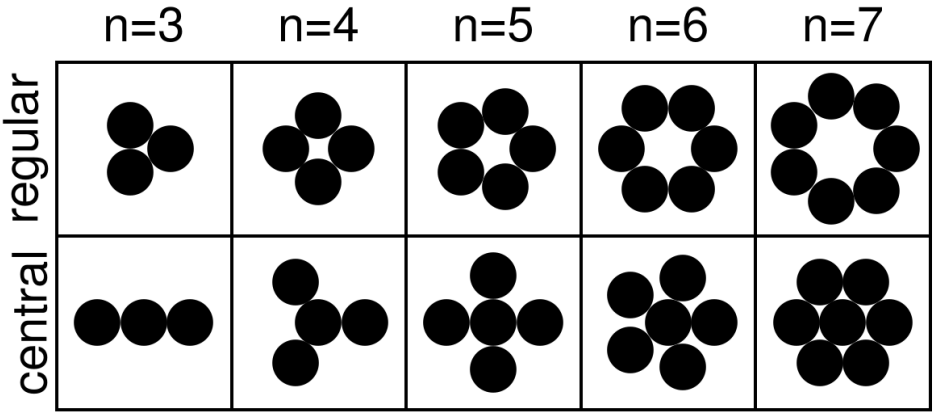

Figure 3.8: Schematic representation of the different aggregate geometries studied. The columns have aggregates with n particles. The top line contains aggregates where the centers of the particles form a regular polygon, in the bottom line the aggregates have a central particle symmetrically surrounded by other particles.

3.3 Aggregates with more grains

To study aggregates with more grains we now assign random charges to the grains according to a Gaussian distribution with average zero and standard deviation one and estimate the fraction of charge distributions that are stable. Two types of aggregate geometry were considered: one geometry type is composed of aggregates where the geometrical center of the grains form a regular polygon, the other geometry type is composed of aggregates with a central grain symmetrically surrounded by other grains, as represented in Fig. 3.8. The charges were generated at random, using the Box–Muller method and for each aggregate geometry the equilibrium of 10^6 different charge combinations where tested using the Metropolis algorithm described above. After evaluating the equilibrium of each aggregate, the aggregates in mechanical equilibrium were filtered according to their mean charge

$$\langle Q_{\text{aggregate}} \rangle = \frac{1}{n} \sum_{i}^{n} Q_i \,, \tag{3.16}$$

where n is the number of particles in the aggregate and Q_i is the charge of grain i, and divided into equally spaced bins of width 0.05. Afterwards, the data was handled to transform the number of occurrences in each bin into a probability density

$$f(Q) = \frac{\#\text{equi}(\text{bin}_i)}{\Delta\text{bin} \times \#\text{equi}}, \tag{3.17}$$

where $\#\text{equi}(\text{bin}_i)$ is the number of aggregates in mechanical equilibrium in bin i, Δbin the width of the bin and $\#\text{equi}$ is the total number of aggregates in mechanical equilibrium.

In Fig. 3.9 are the histograms of the probability density of aggregates in mechanical equilibrium $f(Q)$, for the various geometries, as function of the mean charge of the aggregate. Assuming that the probability density follows a Gaussian distribution with mean zero, it is possible to determine the standard deviation of the distribution

$$\sigma_{\text{equi}} = \sqrt{2\pi}\, \max\{f(Q)\}, \tag{3.18}$$

where $\max\{f(Q)\}$ corresponds to the maximum probability density. The red line corresponds to the plot of the adjusted Gaussian. Notice that the standard deviation of the adjusted Gaussian, σ_{equi} is always

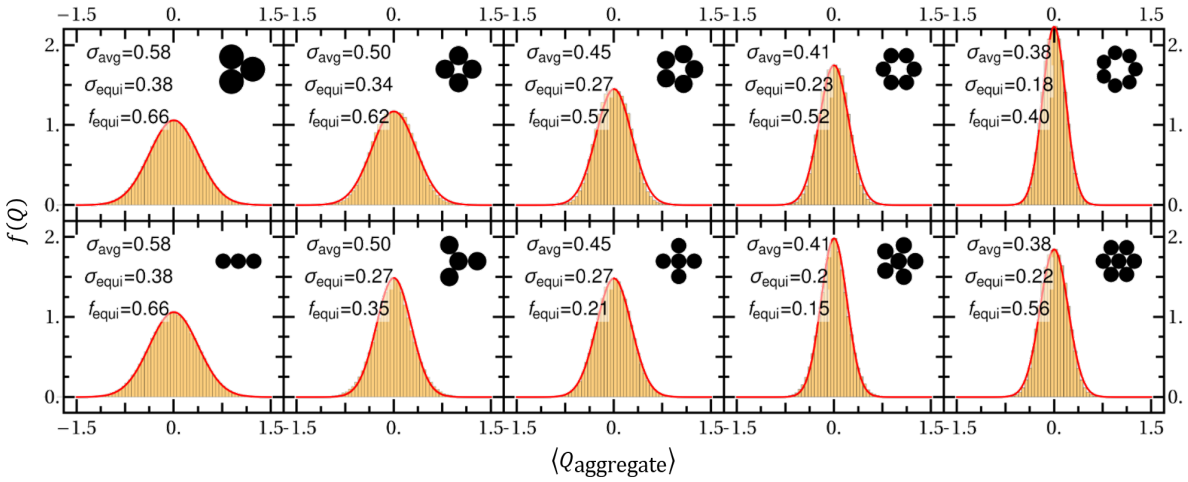

Figure 3.9: Histograms of the density of aggregates in mechanical equilibrium $f(Q)$ as function of the mean charge and the geometry of the aggregate. The insets contain information about the aggregate geometry, the standard deviation of the charge of the aggregates, Eq. (3.19), the adjusted standard deviation, Eq. (3.18) and the fraction of aggregates in mechanical equilibrium, Eq. (3.20). In red is the probability density function of a Gaussian distribution with standard deviation σ_{equi}.

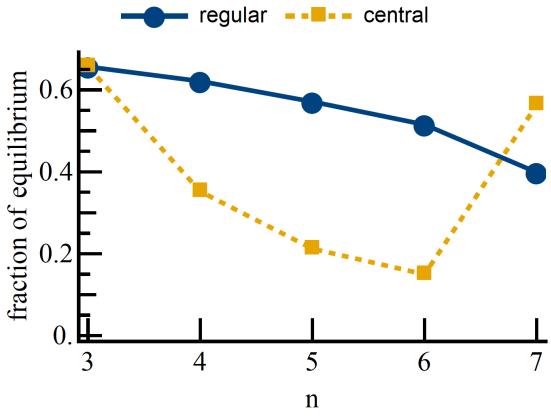

Figure 3.10: Fraction of aggregates in mechanical equilibrium for each aggregate geometry as function of the aggregate size.

smaller than the standard deviation of the Gaussian that describes the average charge of all aggregates, given by the standard deviation of the mean

$$\sigma_{\mathrm{avg}} = \frac{1}{\sqrt{n}}\,, \tag{3.19}$$

as seen on the insets of Fig. 3.9. Thus, low average charge favors the equilibrium of the aggregates.

The fraction of aggregates that are in mechanical equilibrium

$$f_{\mathrm{equi}} = \frac{\#\mathrm{equi}}{\#\mathrm{aggregates}} \tag{3.20}$$

is used to compare aggregate geometries. This quantity is plotted in Fig. 3.10. The probability of finding an aggregate in mechanical equilibrium, in general, decreases with the number of grains. But compact configurations, like the regular configuration with $n = 3$ or the central one with $n = 7$, have higher fractions of aggregates in mechanical equilibrium.

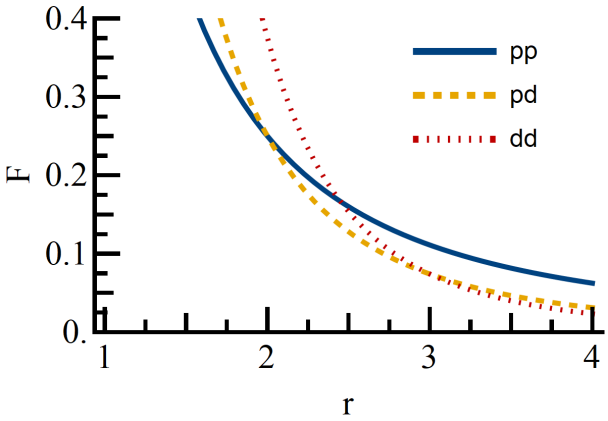

Figure 3.11: Plot of the force (in units of k_e) between two point charges, line in blue, between a point charge and a dipole, dashed line in orange, and between two dipoles, dotted line in red, as function of the distance between them. The point charges are unitary, and the dipole moments are unitary and aligned.

3.4 Higher order terms

A possible follow up is to consider higher order terms of the multipole expansion. Considering all grains with a dipole moment we now have two more degrees of freedom for each grain: the dipole magnitude and dipole orientation. Besides the problem of designing an effective algorithm to run over the configuration space another problem exists, the interaction between dipoles can always be made attractive. Thus, studying this case becomes irrelevant. Let us consider a dipole with moment $\vec{p}$ thus it produces an electric field given by

$$\vec{E}(\vec{x}) = k_e \frac{3\,(\vec{p}\cdot\hat{x})\,\hat{x} - \vec{p}}{\|\vec{x}\|^3}, \tag{2.10}$$

where $\vec{x}$ is the position vector with origin at the dipole center, $\hat{x}$ the normalized vector and k_e the Coulomb constant. Let us consider that the dipole is always aligned with $\vec{x}$ thus simplifying the expression

$$\vec{E} = k_e \frac{2\vec{p}}{\|\vec{x}\|^3}. \tag{3.21}$$

Under an electric field a dipole suffers a force given by

$$\vec{F} = \vec{p}\cdot\nabla\vec{E}. \tag{2.13}$$

Combining Eq. (2.6) and (2.13) the force acting on a dipole due to a point charge q is

$$\vec{F}_{pd} = k_e \frac{2Q\vec{p}}{\|\vec{r}\|^3}. \tag{3.22}$$

Combining Eq. (3.21) and (2.13) we obtain the force between two aligned dipoles with moment $\vec{p}$ as

$$\vec{F}_{dd} = k_e \frac{6\,(\vec{p}\cdot\vec{p})\,\hat{r}}{\|\vec{r}\|^4}. \tag{3.23}$$

The numerical results for Eqs. (3.22), (3.23) and the expression of the force between two unitary point charges, Eq. (2.7), are represented in Fig. 3.11. Because the force between a dipole and a point charge or between two dipoles depends on r^{-3} and r^{-4}, respectively, at short distances the relevant interaction

involves the dipole moment. Thus, given the freedom of choosing the dipole moment and the location of the center of the multipole expansion we can design a system with the dipole interaction as the dominant interaction between grains, thus solely defining the aggregate equilibrium.

3.5 Final remarks

By considering the interaction between virtual charges whose location is related to the charge distribution of particles we found that charge heterogeneity plays a key role in the mechanical equilibrium of aggregates of charged particles. The location of the virtual charges was determined using an implementation of the Metropolis algorithm. We show that the equilibrium of a three particle aggregate can be described using a 1D model. Finally, we found that the mechanical equilibrium of the aggregates is related to its geometry and to the mean charge of the aggregate.

Chapter 4

Aggregates of dielectric spheres

Grains are dielectric materials so they polarize in the presence of an electromagnetic field. This property can result in interesting electrostatic interactions like movement of zero-charge particles under an electric field. In this chapter we will investigate the role of polarization on the stability of aggregates of dielectric particles.

4.1 Model

To investigate electrostatic forces on aggregates as a function of their size, we consider spherical dielectric particles with the same radius R and permittivity ε_p, surrounded by a medium of permittivity ε_0, as illustrated in Fig. 4.1. We evaluate increasing numbers, n, of particles as shown, where for $n \leq 7$, the particles are placed symmetrically around a central particle. For $n > 7$ complete shells of particles are layered concentrically as shown. We fix the charge of the surrounding particles at Q_0 each and define the single central particle to have charge Q_c. For our purposes, we take charge to be distributed uniformly on each particle and we evaluate forces on each particle by solving the Poisson equation [21, 28] for the electrostatic potential V

$$\nabla \cdot [\kappa(\vec{x}) \nabla V(\vec{x})] = -\frac{\rho(\vec{x})}{\varepsilon_0} \,, \tag{2.21}$$

where ρ is the charge density, and $\kappa(\vec{x})$ is the dielectric constant that is one in the medium and is $\kappa = \varepsilon_p/\varepsilon_0$ inside the particles.

All variables are made dimensionless by measuring distances in units of R, charges in units of Q_0, dielectric constants in units of ε_0, and electrostatic forces in units of $Q_0^2/\left[4\pi\varepsilon_0(2R)^2\right]$. Accordingly, all surrounding particles are of unitary charge and the central particle has charge $Q = Q_c/Q_0$. The electric field relates to the electrostatic potential $\vec{E} = -\nabla V$ thus

$$\kappa \nabla \cdot \vec{E} = \rho_f - \nabla\kappa \cdot \vec{E} = \rho(\vec{x}) + \rho_p(\vec{x}) \,, \tag{4.1}$$

where $\rho_p(\vec{x}) = -\nabla\kappa(\vec{x}) \cdot \vec{E}(\vec{x})$ is the polarization charge density. For particle permittivity ε_p, equal to vacuum permittivity, ε_0, the polarization charge density is zero. But when ε_p is different from ε_0, polarization charges arise that alter the electric field, and consequently forces between particles.

At the boundary, $\partial\Omega$, of each particle we impose

$$\begin{aligned} &V_{\text{in}}(\vec{x}) = V_{\text{out}}(\vec{x}) \\ &\vec{n} \cdot (\kappa \nabla V_{\text{in}}(\vec{x}) - \nabla V_{\text{out}}(\vec{x})) = \sigma \end{aligned} \quad \text{for } \vec{x} \in \partial\Omega \,, \tag{4.2}$$

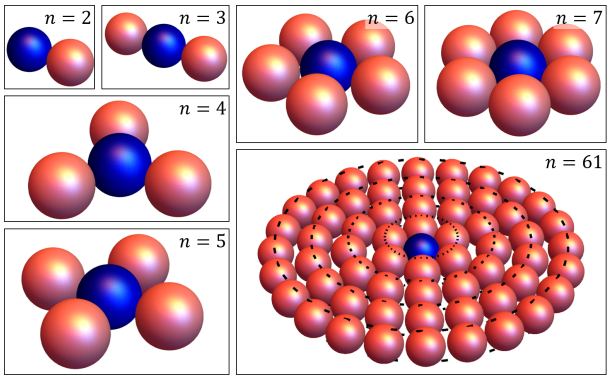

Figure 4.1: Schematics of the aggregates considered here, for numbers, n, of particles indicated. Dielectric spheres have the same radius R and permittivity ε_p. The charge of the central sphere (blue) is Q_c and the surrounding spheres (red) have fixed charge Q_0 each.

where $\vec{n}$ is the unitary vector normal to the particle surface, σ is the surface charge density of the particle and the subscripts in and out denote the potential inside and outside the particle. Notice that when $\kappa = 1$ the permittivity of the medium equals that of the particles, and $\rho_p = 0$.

Far from the particles the electrostatic potential is dominated by the monopole term. Thus, we consider that at the asymptotic boundary S_{asymp}, defined as a spherical shell of radius $R_{\max} = 20R$, the electrostatic potential is

$$V(\vec{x}) = \sum_i \frac{q_i}{|\vec{x}_i - \vec{x}|} \quad \text{for } \vec{x} \in S_{\text{asymp}}, \tag{4.3}$$

where we sum over all particles i with charge q_i and center at $\vec{x}_i$.

As discussed in chapter 2, the force that acts on each particle is obtained by integrating the Maxwell stress tensor [21] over its surface $\partial\Omega$, *i.e.*

$$\vec{F} = \iint_{\partial\Omega} \left[\vec{E} \otimes \vec{E} - \frac{1}{2} \left(\vec{E} \cdot \vec{E} \right) \mathbf{I} \right] \vec{n} dS, \tag{2.9}$$

where $\otimes$ is the dyadic product and $\mathbf{I}$ is the identity matrix. Following Ref. [14], the radial component of the force acting on a surrounding particle due to the central one is given by

$$\begin{aligned} F_r = & \frac{\kappa + 2}{\kappa - 1} \frac{1}{R} a_1 + \\ & + \frac{1}{\kappa - 1} \sum_{n=1}^{\infty} \left[(n+1)(\kappa + 1) + 1 \right] a_n a_{n+1} \end{aligned} \tag{2.35}$$

where a_i represents an infinite sum that is linear with respect to Q. Thus, the radial component of the electrostatic force F_r acting on a surrounding particle relates to the charge of the central particle according to a second order polynomial [24]

$$F_r(Q) = \alpha Q^2 - \beta Q + \gamma, \tag{2.36}$$

where the constant β define the Coulomb interaction (first term in Eq. (2.35)), and the constants α and γ define the force due to particle polarization. Here the coefficients of Eq. (2.36) are determined numerically by least square fitting the data obtained for different charge values in the range $Q \in [-10, +10]$.

The calculation of the electric field in the presence of dielectrics is not trivial and current analytical solutions are very limited, usually involving simple electric fields or systems with few particles, thus we

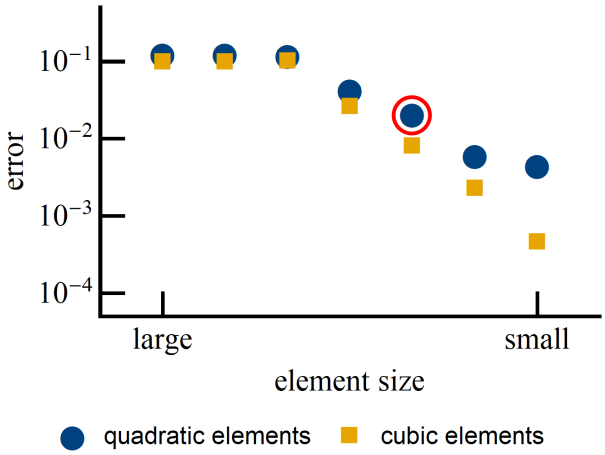

Figure 4.2: Plot of the error as function of the element size for elements described by a second order polynomial (blue circles) and a third order polynomial (yellow squares). The error is given by the relative difference between Coulomb's law (expected value) and the values obtained by solving Poisson's equation. The point inside the red circle corresponds to the mesh parameters chosen.

will use numerical methods to solve Eq. (2.21).

4.2 Finite element methods

The spatial dependence of the electrostatic potential and the electrostatic forces are calculated with the finite element method using COMSOL Multiphysics® software [29,30]. A summary of the finite element method implementation is in Appendix A. The system is divided into a mesh of tetrahedral elements whose size is varied across the system according to the accuracy needed. On the particle boundary, where the accuracy needs to be the highest to calculate the electrostatic forces accurately, the elements are the smallest. On the boundary, where less a accurate field is required, are the largest. The function that describes the potential in each element also has an impact on the accuracy of the electrostatic field, polynomials were used. The impact of the element size and of the type of element was studied by calculating the force between two spheres with unitary radius, with permittivity ε_0, thus no polarization, and with charges $Q_1 = +1$ and $Q_2 = +2$. The relative difference between the magnitude of the determined force and the theoretical one, given by Coulomb's law (2.7)

$$F = k_e \frac{Q_1 Q_2}{r^2}, \tag{4.4}$$

is plotted in Fig. 4.2. For future simulations it was chosen elements that on the particle boundary are smaller than $0.4R$ and on the boundary are larger than $0.72R$. It was chosen quadratic elements to describe the potential

$$\begin{aligned} V(x,y,z) = a_1 + a_2 x + a_3 y + a_4 z + \\ + a_5 xy + a_6 xz + a_7 yz + \\ + a_8 x^2 + a_9 y^2 + a_{10} z^2, \end{aligned} \tag{4.5}$$

meaning there are 10 coefficients a_i per element to be determined. As a result, the force between the two particles only differs 2% from the theoretical one, blue dot inside the red circle in Fig. 4.2.

To solve the linear system associated with the mesh and determine the coefficients, the MUMPS [31] solver was used. A solution to the potential is found when the error estimate, related to the relative

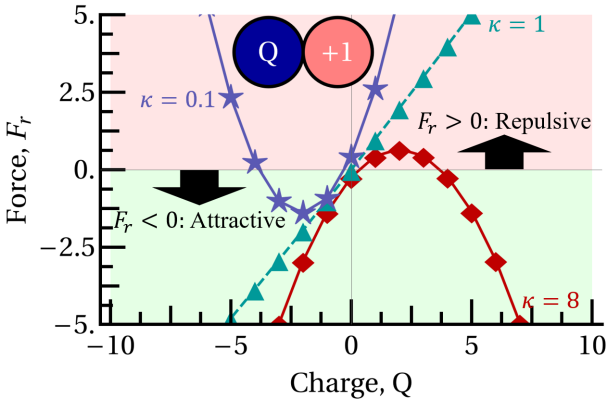

Figure 4.3: Electrostatic force F_r acting on the right-hand particle (of unitary charge) as function of charge Q of the left-hand particle, for $\kappa = 1$ (triangles, red), $\kappa = 8$ (diamonds, green) and $\kappa = 0.1$ (stars, purple). The lower half-plane defines attractive forces between the pair of particles *i.e.*, $F_r < 0$ (shaded green).

residue of the linear system according to Ref. [32], is smaller than 10^{-3}.

4.3 Attraction between like-charge particles

Let us first consider the case of two aggregated particles, as studied in detail by Feng in Ref. [17]. Figure 4.3 shows the radial component of the electrostatic force acting on the particle with unitary charge (red) as a function of the charge Q, of the blue particle. Results for three dielectric constants are shown, $\kappa = 1$, $\kappa = 8$ and $\kappa = 0.1$. For $\kappa = 1$, the interaction between particles follows Coulomb's law

$$F_r = \frac{Q}{4\pi\varepsilon_0(2R)^2}\,, \tag{4.6}$$

so, the attractive force between the particles scales linearly with Q — *i.e.* $\alpha = \gamma = 0$ in Eq. (2.36). In this case, the aggregate coheres only if the particles have charges of opposite sign. By contrast, given the appropriate conditions, for $\kappa = 8$ (*i.e.* $\varepsilon_p = 8\varepsilon_0$) and $\rho_p \neq 0$, the aggregate coheres for particles with like-charges. In fact, ρ_p increases with the strength of the electric field and, consequently, for sufficiently large Q, polarization charges dominate the electrostatic interaction and even same-sign particles can attract, as can be seen in Fig. 4.3 for $Q > 3.7$. Notice that the aggregate is cohesive for $Q = 0$: this is the case of dielectrophoresis on a neutral particle. For $\kappa = 0.1$ the opposite happens, different sign charges can repel for $Q < -3.9$. Since the dielectric constant is smaller than one, polarization charges, that shield the Coulomb interaction, appear on the medium rather than inside the particles.

4.3.1 Three grain aggregates

Before presenting the study of the stability of the aggregates in Fig. 4.1, let us study the impact of the polarization on the stability of an aggregate composed of three spherical grains whose centers form an equilateral triangle, studied in detail in chapter 3. The three grains have a dielectric constant κ and charge Q_0, Q_1 and Q_2 distributed homogeneously on the grain surface. Aggregate is in mechanical equilibrium whenever all forces acting on the grains point towards another one, as described in detail in the beginning of chapter 3, thus the charges can be rescaled according to Q_0 and so $q_1 = Q_1/Q_0$ and $q_2 = Q_2/Q_0$.

Like before, the various charge combinations that allow for the aggregate to cohere are represented in a two-parameter diagram, in Fig. 4.4. In yellow is the case with $\kappa = 1$, *i.e.* no polarization. All the charge combinations that result in an aggregate in mechanical equilibrium are in the second and fourth quadrant,

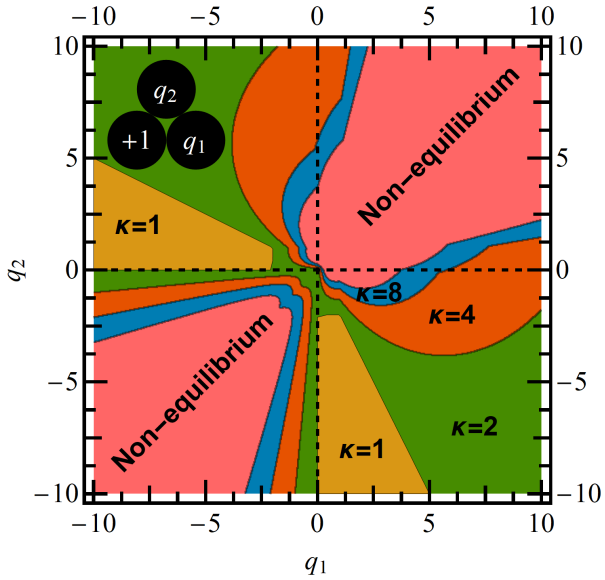

Figure 4.4: Two parameter stability diagram of an aggregate composed of three spheres for different values of dielectric constant κ. The pink regions represent combinations of the charge q_1 and q_2 where stability was not found for any dielectric constant. The yellow region represents the charge combinations where stability is possible for $\kappa = 1$. The green region, in conjunction with the yellow, stability is possible for $\kappa = 2$. For the orange, green and yellow region stability is found when $\kappa = 4$. And finally, for all the regions, except the pink one, stability is possible for $\kappa = 8$.

as derived previously, see section 3.2. When polarization is present, $\kappa = \{2, 4, 8\}$, the number of charge combinations that result in an aggregate in mechanical equilibrium increases due to the dielectrophoretic forces. In fact, when the conditions are appropriate the dielectrophoretic interaction is the dominant one and so aggregates of solely positive charges are possible, see first quadrant for $\kappa = \{4, 8\}$.

4.4 Circular aggregates

The stability of the aggregates in Fig. 4.1 can be assessed by determine the radial component of the force on an outer (red) particle, if the radial component of the electrostatic force is negative the aggregate coheres.

Figure 4.5 shows the limits of cohesion of aggregates of up to seven particles for several values of dielectric constant. Cohesion (*i.e.*, all particles are attracted) is defined by two limits; in the region between the curves, shaded for $\kappa = 8$, the outermost particles experience net outward radial force. Due to the aggregate symmetry, the radial component of the force is the same for all of the outermost particles. For the lower limit, Q is negative, (except for $n = 2$ which we have already discussed), thus the surrounding particles are attracted to the central one due to a combination of Coulomb and polarization forces. Note that above the upper curves, all particles have the same charge sign, thus polarization is responsible for cohesion of the aggregate. By contrast, since polarization grows with the permittivity, the minimum value of Q for which the aggregates are cohesive decreases with κ.

Evidently aggregates with eight or fewer particles can be made electrostatically cohesive by the presence of a strongly charged central particle. To explore larger particle numbers, we simulate successive layers of particles as sketched in the insets to Fig. 4.6. In the body of this figure, we show the dependence of the limits of cohesion on aggregate size up to $n = 61$. The behavior here is similar to that seen for smaller aggregates, except that the magnitude of the central charge by necessity grows with the size of the aggregate. This is easily understood: by symmetry, charges on each layer of surrounding

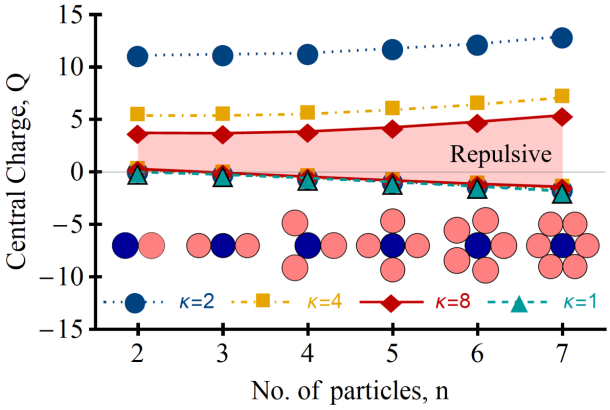

Figure 4.5: Plot of the limits for mechanical equilibrium, corresponding to the zeros of Eq. (2.36), as function of the size, n, of aggregates for different dielectric constants (values shown to the right of each curve). Particle arrangements shown beneath each value of n. In the region between the curves, shaded for $\kappa = 8$, the outermost particles experience a net outward radial force; outside the curves, all particles are radially attracted.

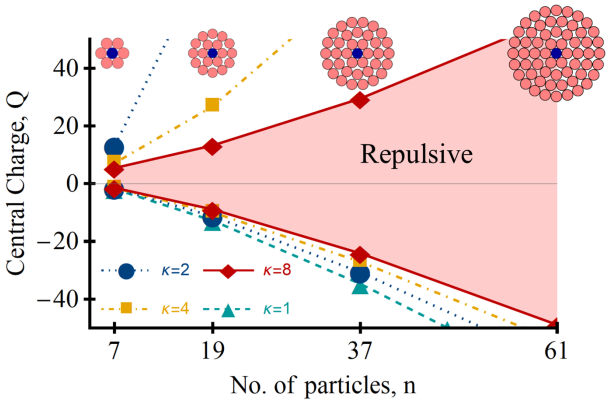

Figure 4.6: Plot of the limits for mechanical equilibrium, corresponding to the zeros of Eq. (2.36), as function of the size, n, of aggregates for different dielectric constants, κ (the corresponding values are close to the values for $n = 37$). In the region between the lines, shaded for $\kappa = 8$, particles are repelled from the aggregate.

particles must be identical, and so forces between surrounding particles are never attractive [16]. Thus, to maintain a cohesive aggregate as more particles are added, attractive forces due to the central particle must grow to compensate for repulsion of surrounding particles. As a consequence, the net charge on the central particle — and so the separation between the upper and lower curves — must grow with the size of the aggregate.

4.5 Experimental aggregates

At the university of Duisburg-Essen, the group of Gerhard Wurm has an experimental set up where charged glass particles, $\kappa \simeq 4$, are dropped onto a micro-gravity chamber with a constant electric field. In this environment they observe aggregates like those in Fig. 4.7. The charges of the particles are represented by a number in the center of the circles. There are some particles, for example in aggregate **b)** and **c)**, whose charge is "$--$" since the results were inconclusive for the charge magnitude. For those particles, the charge was assumed to be $\pm 10^5$e. For aggregates **a)**, **c)** and **e)** the intensity of the external electric field was 42×10^3 V/m, for the remaining aggregates, **b)**, **d)** and **f)** the intensity was 83×10^3 V/m. For all aggregates the electric field points in the direction $-\vec{e}_z$, thus in Fig. 4.7 it points downwards. The stability of those aggregates is not trivial since they are mainly composed of charges of

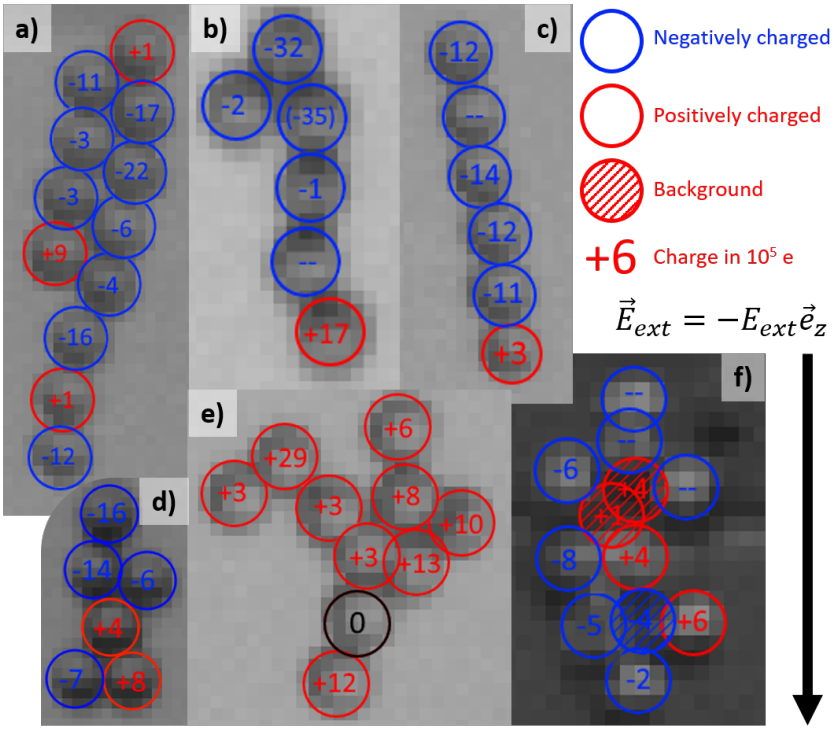

Figure 4.7: Aggregates of charged grains obtained by the group of Gerhard Wurm from the university of Duisburg-Essen. The value inside circles represents the determined charge values. Red values correspond to positive charges and the blue ones to negative charges. The cases were experimental adversities impeded the charge measurement are marked with "−−". The arrow represents the direction of the external field with magnitude E_{ext}.

the same sign, in particular aggregate **e)** only contains positive charges, thus the Coulomb interaction is repulsive for most of the particle pairs.

The positions of the particles of aggregates **a)**, **b)**, **c)** and **d)** were determined assuming that all the particles lay on the same plane and the forces were determined by solving Poisson equation. Since the aggregates have an elongated shape, the asymptotic boundary S_{asymp} is a cylinder, instead of a sphere, with the axis aligned with the electric field and height L. The stability is found whenever all the forces point towards another particle or towards a gap smaller than the particle diameter, see chapter 3 for more details. As example, figure 4.8a has represented cluster **d)** with the normalized forces determined. In gray are the particles whose net force does not obey the stability condition. As can be seen, the net force on the particle with charge -32 points away from the aggregate, thus it will lose contact with the remaining particles.

The experimental set up has an external electric field, and so particle polarization is larger. As established in section 2.1.1, there is no net force on a neutral dielectric particle under a constant electric field, but since polarization is increased, the interaction between particles changes. To solve the Poisson equation with the external electric field, the boundary conditions on the asymptotic boundary were changed. Since the electric field is the negative ratio of the potential difference with the distance, as in Eq. (2.2), to obtain a constant electric field in the z direction the boundary conditions are

$$\begin{aligned} V(\vec{x}) &= 0 \qquad && \vec{x} \in \text{cylinder bottom}, \\ V(\vec{x}) &= E_{\text{ext}} L \qquad && \vec{x} \in \text{cylinder top}, \\ V(\vec{x}) &= E_{\text{ext}} z \qquad && \vec{x} \in \text{cylinder sides}, \end{aligned} \tag{4.7}$$

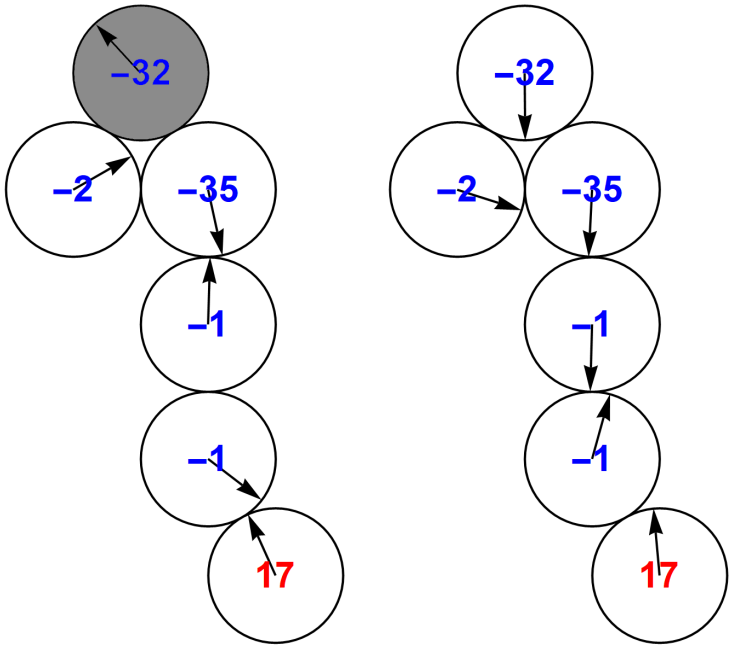

(a) $\vec{E}_{\text{ext}} = 0\ \vec{e}_y \text{V/M}$ (b) $\vec{E}_{\text{ext}} = -83 \times 10^3\ \vec{e}_y \text{V/M}$

Figure 4.8: Normalized force vectors obtained by solving Poisson's equation for aggregate **b)**. The value of the charges is represented by a number in the center of each particle, blue for negative charge and red for positive. The external electric field $\vec{E}_{\text{ext}}$ points downwards. Gray circles correspond to particles whose net force does not follow the stability condition.

where L is the height of the cylinder and E_{ext} is the magnitude of the electric field. The force acting on the particle due to the external field was subtracted from the net force, according to Eq. 2.7 thus, only the interaction between particles is considered. With the electric field, all the forces acting on the particles point towards another one, see figure 4.8b, thus the aggregate stability is found.

From the tested aggregates half of them, aggregates **b)** and **c)**, are in mechanical equilibrium under the external electric field. Although the remaining two, aggregates **a)** and **d)**, are not in mechanical equilibrium, most of the forces obey the stability criteria. But notice that two assumptions made may change that result: **i)** we assumed all particles to be in the same plane and **ii)** we considered particles with homogeneous charge distribution. Regarding the first one, a small change in the position of the charges can significantly change the force because of the external electric field. About the second assumption, in chapter 3 we found that charge heterogeneity can significantly change the stability of aggregates.

4.6 Final remarks

We have numerically solved the Poisson equation for aggregates of dielectric particles. We have confirmed that a central particle can attract large numbers of surrounding dielectric particles — including particles all of the same sign — provided that the charge on the central particle is significantly larger than that on its neighbors. The mechanism at work is simply that the induced polarization on the surrounding particles can overcome Coulombic repulsion. This mechanism is responsible for the mechanical equilibrium exhibit by aggregates of charged particles obtained in laboratory conditions. The work of this chapter has resulted in a publication that is now under evaluation [33].

Conclusion

We have investigated the impact of electrostatic interactions on the mechanical equilibrium of aggregates using numerical and analytical work. Two interactions were studied: the interaction between heterogeneous charged particles and the interaction between dielectric particles.

Regarding the first one, the numerical work shows that it is possible for electrostatic interactions to keep three grains on an aggregate in contact. Furthermore, the study reveals that an uneven charge distribution on the surface of the grains can play a crucial role in keeping the grains in contact. Analytical methods helped explaining the cohesion of the above mentioned two-dimensional aggregate based on a 1D model.

In conjunction to the uneven charge distribution, the numerical work also shows that the geometry of the aggregates is also a relevant parameter on the cohesion of the aggregates. The compactness of the aggregate increases the odds of finding an aggregate in mechanical equilibrium.

These findings can improve the understanding of the formation of millimeter-sized grains observed in the outer space, whose charge have a heterogeneous distribution since their charge must come from collisional charging.

For aggregates of dielectric particles, we have numerically solved the Poisson equation. We showed that particle polarization can enhance the effects of uneven charge distribution in the stability of aggregates of three grains.

We have confirmed that a central particle can attract large numbers of surrounding dielectric particles — including particles all of the same sign — provided that the charge on the central particle is significantly larger than that on its neighbors. The mechanism at work is simply that the induced polarization on the surrounding particles can overcome Coulombic repulsion.

We note in closing that the essential feature that distinguishes cohesive from non-cohesive aggregates is therefore the extent of charge heterogeneity present. Our simulations were by design centrally symmetric, and so cohesive aggregates are characterized by strong variation in radial charge distribution. This could be viewed as concluding that a single highly charged particle can attract large numbers of weakly charged particles — and so we predict a highly charged particle can permit planetesimals or industrial agglomerates to grow through the intermediate size range mentioned in the introduction.

More generally, our central finding is that electrostatic sticking is governed by strong heterogeneity in charge. We observe that real particles are seldom symmetrically charged [34] or arranged [35] and, to understand real aggregate formation, deeper analysis of both charged particle arrangements and charge distributions within particles is called for.

Bibliography

[1] Amit Mehrotra, Fernando J. Muzzio, and Troy Shinbrot. Spontaneous separation of charged grains. *Physical Review Letters*, 99(5):58001, 2007.

[2] Gregory Hendrickson. Electrostatics and gas phase fluidized bed polymerization reactor wall sheeting. *Chemical Engineering Science*, 61(4):1041–1064, 2006.

[3] Y Tian and P Mehrani. Effect of particle size in fluidization of polyethylene particle mixtures on the extent of bed electrification and wall coating. *Journal of Electrostatics*, 76:138–144, 2015.

[4] H. Kent Bowen. Ceramics as engineering materials: Structure-property-processing. *MRS Online Proceedings Library Archive*, 24, 1983.

[5] Jack J. Lissauer. Planet formation. *Annual Review of Astronomy and Astrophysics*, 31:129–174, 1993.

[6] Jürgen Blum and Gerhard Wurm. The Growth Mechanisms of Macroscopic Bodies in Protoplanetary Disks. *Annual Review of Astronomy and Astrophysics*, 46(1):21–56, 2008.

[7] K. L. Johnson, K Kendall, and A. D. Roberts. Surface energy and the contact of elastic solids. *Proceedings of the Royal Society of London A: Mathematical, Physical and Engineering Sciences*, 324(1558):301–313, 1971.

[8] B V Derjaguin, V M Muller, and Yu.P Toporov. Effect of contact deformations on the adhesion of particles. *Journal of Colloid and Interface Science*, 53(2):314–326, 1975.

[9] Andras Zsom, Chris W. Ormel, Carsten Güttler, Jürgen Blum, and C. P. Dullemond. The outcome of protoplanetary dust growth: pebbles, boulders, or planetesimals? - II. Introducing the bouncing barrier. *A&A*, 513:A57, 2010.

[10] Thorben Kelling, Gerhard Wurm, and Marc Köster. Experimental study on bouncing barriers in protoplanetary disks. *Astrophysical Journal*, 783(2):111, 2014.

[11] Maximilian Kruss, Jens Teiser, and Gerhard Wurm. Growing into and out of the bouncing barrier in planetesimal formation. *A&A*, 600:A103, 2017.

[12] Frank Spahn and Martin Seiβ. Charges dropped. *Nature Physics*, 11:709, jul 2015.

[13] Jürgen Blum. Grain growth and coagulation. *Astrophysics of dust*, 309(1985):369–391, 2004.

[14] Yoji Nakajima and Takashi Sato. Calculation of electrostatic force between two charged dielectric spheres by the re-expansion method. *Journal of Electrostatics*, 45(3):213–226, 1999.

[15] Thomas B. Jones. Dielectrophoretic force calculation. *Journal of Electrostatics*, 6:69–82, 1979.

[16] Jian Qin, Jiyuan Li, Victor Lee, Heinrich Jaeger, Juan J. de Pablo, and Karl F. Freed. A theory of interactions between polarizable dielectric spheres. *Journal of Colloid and Interface Science*, 469:237–241, 2016.

[17] James Q. Feng. Electrostatic interaction between two charged dielectric spheres in contact. *Physical Review E*, 62(2):2891–2897, 2000.

[18] Zecheng Gan, Huanxin Wu, Kipton Barros, Zhenli Xu, and Erik Luijten. Comparison of efficient techniques for the simulation of dielectric objects in electrolytes. *Journal of Computational Physics*, 291:317–333, 2015.

[19] Chamkor Singh and Marco G. Mazza. Early-stage aggregation in three-dimensional charged granular gas. *Physical Review E*, 97:022904, 2017.

[20] Ryuta Yoshimatsu, Nuno A.M. Araújo, Gerhard Wurm, Hans J. Herrmann, and Troy Shinbrot. Self-charging of identical grains in the absence of an external field. *Scientific Reports*, 7:1–11, 2017.

[21] David Jeffery Griffiths. *Introduction to Electrodynamics*. Prentice Hall, 3rd edition, 1999.

[22] Manuel Fiolhais, Lucília Brito, and Constança Providência. *Campo Eletromagnético*. Mc Graw-Hill, 1999.

[23] Andreas Ammitzbøll, Janosch Rauba, and Marco Schultz. The dielectrophoretic force on dielectric spherical objects. Technical Report June, Department of Micro and Nanotechnology Technical University of Denmark, 2006.

[24] Thomas B. Jones. *Electromechanics of Particles*. Cambridge University Press, 1995.

[25] Ramu Anandakrishnan, Charles Baker, Saeed Izadi, and Alexey V. Onufriev. Point Charges Optimally Placed to Represent the Multipole Expansion of Charge Distributions. *PLoS ONE*, 8(7):1–13, 2013.

[26] Charles-Augustin de Coulomb. Sur une application des regles de maximis et minimis a quelques problemes de statique relatifs a l'architecture. *Memoires de Mathematique et de Physique par divers Savants*, 7:343–382, 1773.

[27] Heinrich Hertz. Ueber die Berührung fester elastischer Körper. *Journal für die reine und angewandte Mathematik*, 92:156–171, 1882.

[28] John D. Jackson. *Classical Electrodynamics*. John Wiley & Sons, Inc., 1962.

[29] COMSOL AB, Stockholm, Sweden. *COMSOL Multiphysics® v. 4.2a*, 1998–2011.

[30] Gilbert Strang. *Computational Science and Engineering*. Wellesley-Cambridge Press, 2007.

[31] Patrick R. Amestoy, Abdou Guermouche, Jean Yves L'Excellent, and Stéphane Pralet. Hybrid scheduling for the parallel solution of linear systems. *Parallel Computing*, 32(2):136–156, 2006.

[32] COMSOL Multiphysics®v. 4.2a. *Reference Guide*. COMSOL AB, Stockholm, Sweden, 2011.

[33] André F. V. Matias, Troy Shinbrot, and Nuno A. M. Araújo. Preprint: Mechanical equilibrium of aggregates of dielectric spheres.

[34] Troy Shinbrot, Brandon Jones, and Pranav Saba. Preprint: Charging at a distance.

[35] Dietrich Wolf, Kolja Jöris, Sebastian Rohde, and Lothar Brendel. Preprint: Effects of charge distributions on particle aggregation.

Appendix A

Finite element method

Partial differential equations are fundamental in the description of physical phenomenon, unfortunately most of the partial differential equations are yet to be solved with analytical methods. The finite element method (FEM) is a numerical method to solve partial differential equations.

We will briefly describe FEM for a 1D problem, for a more in-depth look we advise the book of Gilbert Strang [30] as well his course on MIT OpenCourseWare. To solve a problem using FEM, the problem domain is approximated by a mesh with n nodes. Using the Galerkin method, the region between mesh nodes, called finite element, is described by functions $\psi_i(x)$, that form a basis, and the approximate solution $u_h(x)$ to the problem is the linear combination of basis function

$$u_h(x) = \sum_i u_i \psi_i(x). \tag{A.1}$$

The basis can be composed of a variety of function with the linear function, also called "hat" function, the simplest example, see Fig. A.1[1]. To determine the coefficients u_i, the partial differential equation is transformed into its weak form. For a 1D problem, the weak form is obtained by multiplying the partial differential equation by a test function $w(x)$ and then the equation is integrated over the domain of the problem, for example $x \in [0, 1]$. In the case of the Poisson equation we have

$$-\nabla \cdot [\kappa(x)\nabla V(x)] = \frac{\rho(x)}{\varepsilon_0} \Leftrightarrow -\int_0^1 \nabla \cdot [\kappa(x)\nabla V(x)]\, w(x)dx = \int_0^1 \frac{\rho(x)}{\varepsilon_0} w(x)dx. \tag{A.2}$$

After integrating by parts, we obtain

$$\int_0^1 [\kappa(x)\nabla V(x)]\, \nabla w(x)dx = \int_0^1 \frac{\rho(x)}{\varepsilon_0} w(x)dx, \tag{A.3}$$

where the second term of the integration by parts disappears by imposing that $[\kappa(x)\nabla V(x)]\, w(x)$ is zero on the boundaries, a condition that naturally arises from the boundary conditions of the problem. The choice of the test functions is arbitrary, we chose the test functions to be the same as the basis functions ψ_i. And so, by combining Eq. (A.1) and (A.3) the problem is discretized and the unknown coefficients u_i can be determined by solving a system of linear equations

$$A\mathbf{x} = \mathbf{b}, \tag{A.4}$$

[1] When the basis is composed of linear functions, the finite element method is the same as the finite difference method.

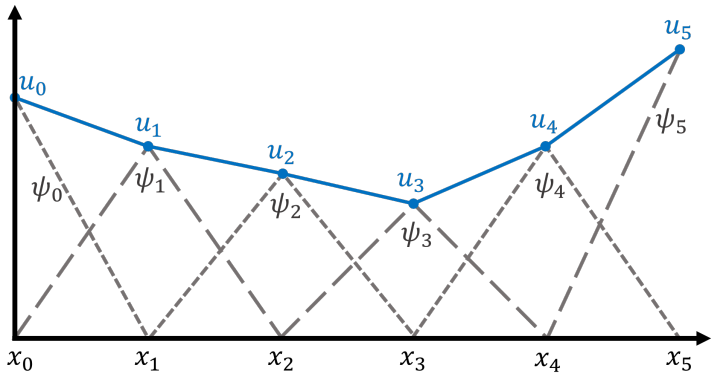

Figure A.1: Example of a function, in blue, approximated by hat functions, in gray. Each hat function ψ_i is composed of two linear functions defined in $[x_{i-1},\ x_i]$ and $[x_i,\ x_{i+1}]$, except on the boundaries where ψ_i is defined by a single linear function. The values on each element are determined by the linear combinations of the hat functions.

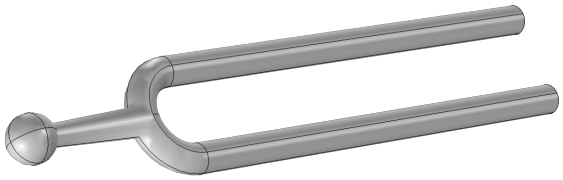

Figure A.2: Example of a possible domain of a problem in COMSOL Multiphysics® software. A model of a tuning fork used to study the vibration modes.

where A is a $n \times n$ matrix, called the stiffness matrix, **b** is a vector of length n related to the boundary conditions and **x** is a vector with the n unknown coefficients. To solve the linear system, a conventional linear system solver can be used like LU decomposition, GMRES or the MUMPS solver.

COMSOL Multiphysics® software [29] is a ready to use implementations of FEM and it provides the tools to work with electrical, mechanical, fluid, and chemical problems, as well to solve a generic partial differential equation. Using COMSOL Multiphysics® software we can manipulate the geometry of the problem, the mesh that approximates the domain, the type of elements, the boundary conditions and additional parameters of the problem as well performing post-processing of the results, including plot creation, result filtering or numerically integration.

We are interested in solving Poisson equation, thus we will focus on the Mathematics module that contains an implementation that solves a generic Poisson equation. The geometry of the problem can be anything from a one-dimensional line to a complex structure in a three-dimensional environment, see figure A.2.

A great level of freedom is also provided by the built-in tools to define the mesh that best suits the problem. The shape and size of the elements as well their density can be controlled across the system. This feature can be useful to adapt the shape of the elements to the geometry of the system, or to obtain a more detailed solution on key regions, like the boundaries. The size of the elements can be controlled using five different parameters: **i)** the maximum and **ii)** minimum distance between nodes inside a region, referred as maximum and minimum element size; **iii)** the maximum element growth that defines the maximum size difference between adjacent elements when going from a region with a finer

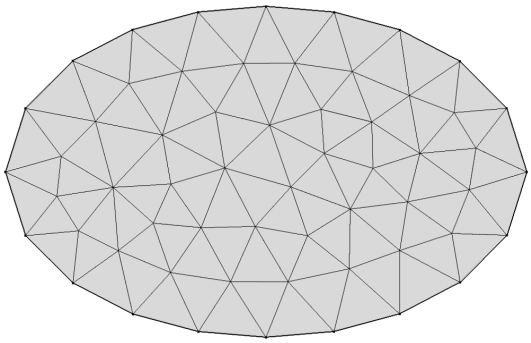

Figure A.3: A coarse mesh for a problem with elliptical geometry.

mesh to one with a coarser mesh; **iv)** the curvature factor is used to control the element size on curved borders; and **v)** the resolution on narrow regions that controls the number of elements in narrow regions. The default parameters for several levels of mesh details can be found in table A.1. In figure A.3 is an example of a coarse mesh for an elliptical domain. The shape of the function basis can be, for example, Lagrange (commonly referred as polynomials), Hermite or others of order one to seven.

The computational demand is mainly dictated by the choice of mesh and elements, a finer mesh and elements of higher order will result in a more precise solution, but more memory and computational time are required. Thus, a balance between precision and computational demand needs to be established.

Finally, to solve partial differential equations it is also required to define the boundary conditions and COMSOL Multiphysics® gives the freedom of choosing between Dirichlet and Newman boundary conditions. Furthermore, it allows for the definition of the boundary conditions in geometric entity of any dimension from a point to a volume.

Table A.1: Default mesh parameters of COMSOL Multiphysics®.

	Maximum element size	Minimum element size	Maximum element growth rate	Curvature factor	Resolution of narrow region
Extremely fine	8.0×10^{-1}	8.00×10^{-3}	1.30	0.2	1.00
Extra fine	1.4×10^{0}	6.00×10^{-2}	1.35	0.3	0.85
Finer	2.2×10^{0}	1.60×10^{-1}	1.40	0.4	0.70
Fine	3.2×10^{0}	4.00×10^{-1}	1.45	0.5	0.60
Normal	4.0×10^{0}	7.20×10^{-1}	1.50	0.5	0.50
Coarse	6.0×10^{0}	1.12×10^{0}	1.60	0.7	0.40
Coarser	7.6×10^{0}	1.60×10^{0}	1.70	0.8	0.30
Extra coarse	1.2×10^{1}	2.16×10^{0}	1.85	0.9	0.20
Extremely coarse	2.0×10^{1}	2.80×10^{0}	2.00	1.0	0.10